



# **Climate co-variability between South America and Southern Africa at interannual, intraseasonal and synoptic scales.**

Yohan Puaud, Benjamin Pohl, Nicolas Fauchereau, Clémence Macron, Gérard Beltrando

## **► To cite this version:**

Yohan Puaud, Benjamin Pohl, Nicolas Fauchereau, Clémence Macron, Gérard Beltrando. Climate co-variability between South America and Southern Africa at interannual, intraseasonal and synoptic scales.. Climate Dynamics, 2017, 48 (11), p. 4029-4050. <10.1007/s00382-016-3318-x>. <hal-01528459>

**HAL Id: hal-01528459**

**<https://hal.science/hal-01528459v1>**

Submitted on 20 Feb 2024

**HAL** is a multi-disciplinary open access archive for the deposit and dissemination of scientific research documents, whether they are published or not. The documents may come from teaching and research institutions in France or abroad, or from public or private research centers.

L'archive ouverte pluridisciplinaire **HAL**, est destinée au dépôt et à la diffusion de documents scientifiques de niveau recherche, publiés ou non, émanant des établissements d'enseignement et de recherche français ou étrangers, des laboratoires publics ou privés.



HAL Authorization

1  
2  
3  
4  
5  
6  
7  
8  
9 **Climate co-variability between South America and Southern**  
10 **Africa at interannual, intraseasonal and synoptic scales**  
11  
12  
13  
14

15 Yohan Puaud<sup>1,2</sup> \*, Benjamin Pohl<sup>1</sup>, Nicolas Fauchereau<sup>3</sup>, Clémence Macron<sup>1</sup>, Gérard Beltrando<sup>2</sup>  
16

17 <sup>1</sup> Centre de Recherches de Climatologie, UMR6282 Biogéosciences, CNRS / université de Bourgogne Franche-  
18 Comté, Dijon, France

19 <sup>2</sup> UMR8586 PRODIG, CNRS / université Paris Diderot, Paris, France

20 <sup>3</sup> National Institute of Water and Atmospheric Research (NIWA), Auckland, New Zealand  
21  
22  
23  
24  
25

26 Puaud Y, B Pohl, N Fauchereau, C Macron & G Beltrando (2017) Climate co-variability  
27 between South America and Southern Africa at interannual, intraseasonal and synoptic scales.  
28 Climate Dynamics, 48, 4029-4050. doi:10.1007/s00382-016-3318-x  
29  
30  
31  
32  
33

34 **\* Corresponding author's address**

35 Dr. Benjamin Pohl

36 Centre de Recherches de Climatologie / Biogéosciences

37 6 boulevard Gabriel - 21000 Dijon - France

38 benjamin.pohl@u-bourgogne.fr

## **Abstract**

This paper investigates and quantifies co-variability between large-scale convection in the South American and Southern African sectors at different timescales (interannual, intraseasonal and synoptic), during the austral summer seasons (November to February) from 1979 to 2012. Multivariate analyses (Canonical Correlation Analysis and Principal Component Analysis) are applied to daily outgoing longwave radiation (OLR, used as a proxy for atmospheric convection) anomalies to extract the principal modes of variability and co-variability in each and between both regions, filtered to consider the appropriate time-scales. At the interannual timescale, results confirm the predominant role of El Niño Southern Oscillation (ENSO), favoring enhanced convection over both southeastern Brazil and northern Argentina on the one hand, and tropical Africa and the western Indian Ocean on the other hand. At the intraseasonal timescale, the leading mode of co-variability is related to modulations of large-scale atmospheric convection over most of South America, and ten days later, tropical Southern Africa. This mode accounts for the impacts of the Madden-Julian-Oscillation (MJO) over these regions: identifying robust co-variability at the intraseasonal timescale between both regions require thus to consider a temporal shift between the two sectors. At the synoptic scale, however, co-variability consists mostly of a synchronous modulation of the large-scale atmospheric convection over the South American and Southern African sectors. This results from the development of concomitant Rossby waves forming a continuous wave train over the South Atlantic in the mid-latitudes, affecting both the South Atlantic and South Indian Convergence Zones. Among the days when convection shows significant anomalies (30% of the total days in each sector), this synchronous mode occurs about 25% of the time, individual Rossby waves modulating convection over one single region only during the remaining 75% events. Another mode of co-variability, involving a single Rossby wave modulating the convection first over the Americas, and four days later over Africa, appears as sensibly weaker than the synchronous mode, suggesting that the “wave train” mode occurs more frequently than the development and propagation of a single wave that could propagate and affect both regions.

## **Key-words**

El Niño Southern Oscillation; Madden-Julian Oscillation; Rossby waves; Co-variability; Atmospheric convection; South Atlantic Convergence Zone; South Indian Convergence Zone.

*This study is dedicated to the memory of Professor Gérard Beltrando.*

## **1. Introduction**

Three main convergence zones (CZ) linking the tropics to the mid-latitudes are found in the Southern Hemisphere (Streten 1973): the South Pacific (SPCZ, northeast of Australia: Vincent 1994), South Atlantic (SACZ, spreading from the Amazonia basin to the southwestern Atlantic Ocean: Liebmann et al. 1999; Carvalho et al. 2004) and South Indian (SICZ, from Southern Africa to the southwest Indian Ocean: Cook 2000) convergence zones. These CZs are associated with significant rainfall, notably during the Southern Hemisphere summer and therefore their variability in space and time (i.e. position, intensity) contribute to modulate large-scale rainfall over their corresponding regions, affecting the livelihoods of millions of people.

As a consequence, many studies have been devoted to improve our understanding of the physical mechanisms responsible for their establishment, and what controls their variability at time-scales ranging mostly from synoptic to interannual. Early studies by Kodama (1992; 1993) suggested that the Southern Hemisphere CZs appear when two necessary conditions in the mid-latitude circulation are satisfied: (i) subtropical jet flows in the subtropical latitudes (30-35°S), and (ii) low-level poleward flows prevail along the western peripheries of the subtropical highs (see also Barreiro et al. 2002). A common denominator identified in all 3 Southern Hemisphere CZs is therefore their association with mid-latitude wave trains, the vorticity centers of which elongate along their equatorward flank, and interact with atmospheric instability to favor deep convection over these regions (Widlansky et al. 2011; Macron et al. 2014; Van Der Wiel et al. 2015).

A fundamental difference however exists between the SPCZ on the one hand and both the SACZ and the SICZ on the other hand. The former originates over what consists largely of open ocean, and continental configuration and orography has been shown to have negligible influence on the SPCZ orientation and intensity (e.g., Van Der Wiel et al. 2015). In contrast, both the SICZ and the SACZ originate from continental landmasses. The SACZ originates in the Amazon basin, and is considered part of the South American Monsoon System (see e.g. Carvalho et al. 2004). Figueroa et al. (1995) showed that diabatic heating over the Amazon and the steep Andean topography are both essential ingredients for the formation of the SACZ, while Lenters et al. (1995) attribute the

formation of the SACZ to the land–sea contrast in the absence of topography and longitudinal Sea Surface Temperature variations (Barreiro et al. 2002). In both views, diabatic heating over the continental landmass is a conditional mechanism for the formation of the SACZ.

The South Indian Convergence Zone (SICZ, Cook 2000) can be considered to correspond to the time-integrated signature of synoptic systems called Tropical Temperate Trough (TTT, see e.g. Todd and Washington 1998; 1999). TTT systems (and by extension the SICZ) appear to be systematically associated with a mid-latitude transient perturbation, interpretable as an atmospheric Rossby wave, coinciding with moisture convergence over tropical southern Africa. The latter is related on one hand to the reinforcement of the so-called Angola low (forming over the Angolan – Zambian region in summertime) that favors flux penetration from the Atlantic basin toward southern Africa on the west and on the other hand to easterly moisture fluxes from the nearby Indian Ocean and Mozambique Channel on the east (Macron et al. 2014). Cook (2000) coins the term “Land-Based Convergence Zones” (LBCZ) to describe both the SACZ and the SICZ and also argues that thermal lows over the land surface is necessary to sustain a root zone for the LBCZs.

Because of the involvement of both tropical and mid-latitudes mechanisms in both the formation, variability and maintenance of the SACZ and SICZ, it is reasonable to surmise that the SACZ and the SICZ, and therefore rainfall variability in the South American and Southern African regions at large, could potentially be connected, both via tropical teleconnection patterns and modes of tropical variability (i.e. the ENSO at interannual time-scales, the Madden Julian Oscillation at intra-seasonal timescales) as well as mid-latitude wave trains. To date however, very little attention has been given to the potential (statistical and physical) relationships between these two regions. Co-variability between the South American and Southern African regions (affected by the SACZ and SICZ respectively), either synchronous or with some temporal lag, could however bear the potential for improved predictability at various time-scales, a perspective of great importance given the dependency of both South American and Southern African economies to rain-fed agriculture (Mason and Jury 1997; Jury 2002; Reason and Jagadheesha 2005).

This issue provides the impetus for this study. In the present paper, we are interested in assessing to what extent large-scale atmospheric convective variability over the African sector is connected to the American region, and whether large-scale convective variability over Southern Africa and

nearby Indian Ocean could be anticipated using South American convection as a predictor. The goals of the present study are to:

(i) assess and quantify climate co-variability between the Southern African and South American regions, either synchronous or lagged, and at three different timescales : interannual, intraseasonal and synoptic;

(ii) analyse whether co-variability between the two regions involves modulation in the location and intensity of the SACZ and SICZ;

(iii) identify associated mechanisms and processes.

To that end, multivariate statistical methods maximizing the variance in each region and the covariance between both regions are applied to a proxy of large-scale atmospheric convection. Atmospheric dynamics and thermodynamics derived from current reanalyses are used to verify that the modes of (co)-variability identified are not merely statistical artifacts and correspond indeed to well-known modes of climate variability affecting these regions on timescales investigated here.

This study is organized as follows. Section 2 presents the data and methodology used for this work. Section 3 documents the results for each timescale (interannual, intraseasonal and synoptic). Section 4 finally summarizes and discusses our main results.

## **2. Data and methods**

### *2.1 Datasets*

Daily tropical convection is estimated through the National Oceanic and Atmospheric Administration (NOAA) interpolated outgoing longwave radiation (OLR) dataset (Liebmann and Smith 1996), available daily on a 2.5 x 2.5 regular grid. The 1979 – 2012 period is considered in this study. Fig. 1 shows the seasonal mean OLR field in austral summer (November through February, NDJF hereafter) over a domain encompassing both the SACZ and the SICZ. In the tropics, OLR is a good proxy for deep atmospheric convection. The most convectively active areas of the region (Amazonia and Congo basins), as well as both CZ, are clearly discernible in Fig. 1.

Monthly SST are obtained from the HadISST dataset (Rayner et al. 2006) on a  $1^\circ \times 1^\circ$  regular grid. Only NDJF seasonal means and anomalies computed for the 1979 – 2012 period are used here. Atmospheric fields are provided by the state-of-the-art European Centre for Medium-Range Weather Forecasts ERA-Interim reanalyses (Simmons et al. 2007; Dee et al. 2011), available every 6 h since 1979 on a  $0.75 \times 0.75^\circ$  regular grid. The fields used in this work are the horizontal (zonal and meridional) wind components at 850 and 200hPa, which are among the most reliable variables since they are directly constrained by data assimilation (refer to Kalnay et al. 1996 for more details).

The state of ENSO is monitored using the Multivariate ENSO Index (MEI, Wolter and Timlin 1993). This bimonthly index, based on both atmospheric and oceanic fields (namely, sea-level pressure, zonal and meridional components of the surface wind, sea surface temperature, surface air temperature, and total cloudiness fraction of the sky), is adequate to describe the coupled nature of the ENSO phenomenon. All the input variables cited above are taken from the International Comprehensive Ocean-Atmosphere Data Set (ICOADS).

The MJO signal is represented by the real-time daily indices developed by Wheeler and Hendon (2004, hereafter referred to as WH04). The indices are the time series of the two leading eigenvectors of a Principal Component Analysis (PCA) of combined daily mean tropical (averaged  $15^\circ\text{N}$ – $15^\circ\text{S}$ ) anomalies of 850 and 200hPa zonal wind (derived from NCEP/NCAR reanalyses, Kalnay et al. 1996) and the NOAA interpolated OLR. WH04 subtracted the annual cycle and the low-frequency variability associated with ENSO before applying the PCA. The indices, denoted real-time multivariate MJO (RMM1 and RMM2), were designed to be used in real time and to capture both the northern winter and summer MJO. RMM1 and RMM2 are approximately in quadrature and describe the average large-scale, eastward-propagating convective and circulation anomalies associated with the MJO.

## *2.2 Methods*

Co-variability between the South American and Southern African regions is documented in this work through Canonical Correlation Analyses (CCA hereafter). CCA can be used to identify the most energetic modes of co-variability between two variables or sets of variables. In this study, CCA is applied on OLR data extracted over the South American and Southern African regions

(see domain definition in Fig. 1). The definition of the South American domain (AM hereafter) is inspired by the anomaly patterns discussed in Carvalho et al. (2004) and more recently Jorgetti et al. (2014). Its counterpart for Southern Africa (AF) is that already used e.g. in Todd and Washington (1999), Fauchereau et al. (2009) or Vigaud et al. (2012). Preliminary tests were made to ensure the robustness of the detected modes of co-variability and their sensitivity to the choice of these domains; particular attention was given to the possible decouplings between the oceanic and continental parts of the South American domain (Carvalho et al. 2002a; 2004; 2011). Results (not shown) reveal a good stability of the main modes. Prior to the CCA decompositions, and depending on the timescale investigated (intraseasonal or synoptic), we used a Butterworth temporal filter to retain characteristics timescales of interest. Additional analyses based on Lanczos or digital filters led to qualitatively similar results and alter none of our conclusions, suggesting weak sensitivity to the filtering procedure (not shown). We also used temporal lags between the two regions to take into account potential propagations of convective anomalies or atmospheric waves from one sector to another. Further details are provided below. In order to further ensure the consistency of the modes of co-variability identified by the CCA, the latter are also compared to the main modes of OLR variability over each region, such as extracted by PCA applied to each domain separately. Results are discussed in the following sections and in the Appendix. In the following, we choose to present only the first mode of co-variability for each timescale. This is because (i) the first mode are clearly distinguishable over other ones (almost two times more co-variance explained compared to the second modes for each timescale), and (ii) the second modes show spatial and temporal patterns that are more ambiguous and less easy to interpret, corresponding to no well-known mode of variability (Appendix) influencing both regions, which questions thus their physical robustness. Finally, the sensitivity to the domain size and location was addressed by a series of preliminary analyses (some of which consisting in separating the oceanic and continental parts of each domain). Results revealed remarkably stable modes of co-variability for the three timescales presented and discussed below.

### 3. Results

#### *3.1 Interannual timescale*



In order to quantify climate co-variability between both domains at the interannual timescale, a CCA is applied in this section on the seasonal mean OLR fields during austral summer (NDJF) from 1979 to 2012. Only the first mode of co-variability extracted from the CCA is described here (Fig. 2). It explains about 42% of the total covariance between the two domains. Associated time series display a strong positive correlation ( $R > 0.75$ ,  $p\text{-value} < 0.01$ ) denoting a clear tendency for seasonal anomalies to occur in phase between the two sectors. They show no or weak autocorrelation (i.e. persistence from one year to another), as estimated by the methodology of Der Megreditchian (1992, which estimates the actual number of degrees of freedom in a given time series), even though they could possibly show a long-term trend towards positive values (not significant for the “AM” time series, only significant at 90% in the African sector according to a Spearman test).

Spatially, the regions of largest loadings (Fig. 2) show:

(i) for the American domain, a meridional dipole between northern Brazil and southeastern Brazil / northern Argentina, the latter region being connected to the Southern Atlantic basin through a NW-SE oriented alignment. The latter is located too far south compared to the typical location of the SACZ such as reported in the studies cited above.

(ii) over the African domain only the southwestern and northeastern parts of the domain (i.e. the southern Atlantic and tropical Indian Oceans) show significant co-variability with American convection, in phase (out of phase) with the southern (northern) pole of the South American dipole discussed above; correlations are not significant over Southern Africa and the SWIO (that is, the climatological location of the SICZ).

Over both sectors, the spatial patterns of this mode of co-variability are strongly reminiscent of regional effects of ENSO on large-scale convective variability in austral summer. Such high co-variability is presumed to result from the common influence of a mode of large-scale climate variability.

At the interannual timescale, ENSO is clearly the dominant mode of variability in the tropics and has been shown to affect significantly both regions. For South America, seasonal dry conditions over northern Brazil and wet anomalies further south are usually observed during El Niño austral summers (Grimm et al. 2000; Cazes-Boezio et al. 2003; Krishnamurthy and Misra 2010). In Africa, El Niño is associated with wet anomalies in Equatorial East Africa (e.g., Nicholson 2015),

northern Madagascar and the adjacent SWIO, contrasting with dry conditions in continental Southern Africa (Fig. 4f). There, regional ENSO effects are non-linear (Reason and Jagadheesha 2005; Fauchereau et al. 2009), as illustrated by the contrasted effects of the very strong 1982-83 and 1997-98 events (e.g., Lyon and Mason 2007; Boulard et al. 2013).

However, the degree to which the SACZ and SICZ *stricto sensu* are modulated by ENSO is open to interpretation. Robertson and Mechoso (2000) suggest that interannual variability of the SACZ is largely independent from ENSO, while Carvalho et al. (2002a) indicate that extreme rainfall events associated with intense convection in the SACZ is modulated by ENSO. Moreover, Carvalho et al. (2004) moreover indicate that a persistent SACZ with a well-defined oceanic (continental) activity is favored during warm (cold) ENSO episodes. Barreiro et al. (2002) also show that part of the SACZ variability is remotely forced by Pacific SSTs, with a response notably consisting of a northeastward shift of the SACZ with associated rainfall anomalies during warm ENSO events. Over Southern Africa, El Niño has been reported to shift eastwards the SICZ. Cook (2001; 2003) proposed that ENSO generates atmospheric Rossby waves in the Southern Hemisphere which could be responsible for such a longitudinal shift, hereby explaining the seasonal droughts typically associated with El Niño events in Southern Africa. In contrast, Nicholson (1997) and Nicholson and Kim (1997) find a predominant oceanic forcing, warm SST anomalies over the Indian Ocean acting to shift convective activity over the SWIO. Misra (2003) partly reconciled these two hypotheses by estimating that the spatial structure of SA rainfall anomalies is mainly dependent on regional Indian Ocean SST, while their amplitude is modulated by large- scale atmospheric Rossby waves.

Concerning interannual co-variability, even though the patterns of Fig. 2 are fairly consistent with the typical signature of ENSO over these regions, it is worth noting that the canonical ENSO pattern over Southern Africa usually shows larger correlations than those found in Fig. 2 (see Fig. 4f and e.g., Lyon and Mason 2007; Fauchereau et al. 2009; Lyon and Mason 2009; Pohl et al. 2009), suggesting first a partial influence of ENSO interfering here with other mechanisms (such as e.g. the seasonal anomalies of the so-called “Angola Low”, invoked in Reason and Jagadheesha 2005 to explain the non-systematic effects of ENSO over the southern tip of the African continent). Second, the correlation coefficient between the time series associated with each domain and the MEI is even slightly higher than that between the two domains, hereby indicating that roughly 60% of their variance linearly relates to the state of ENSO. Third, a partial correlation between the

time series derived from the CCA after removing the influence of ENSO decreases to 0.36 (not shown; still significant at the 98% level), denoting a dominant (but not exclusive) role of ENSO at this timescale.

Some insights on the mechanisms responsible for this mode of co-variability are proposed in the following. The correlations between mean horizontal wind at 200hPa and 850hPa and OLR are displayed in Figs. 3-4. Results presented here corroborate Boulard et al. (2013): ENSO acts to shift polewards the mid-latitude westerlies (which are thus weakened at the subtropical latitudes and enhanced south of 50°S). Negative correlations with the OLR at the subtropical latitudes (Fig. 4f) suggest larger cloud fractions during El Niño events, although the accuracy of OLR as an indicator of upper-layer cloud cover (probably both stratiform and convective) is reduced there compared to the tropics. Very similar wind and OLR correlations (of opposite sign) are obtained with the AM and, to a lesser extent, the AF time series. Similarities with the MEI are stronger for the AM series, consistently with Fig. 2. Although all time series lead to very similar variability patterns over the American sectors, clear and spatially-coherent convective signals over Southern Africa are only found for the AF time series. The MEI is associated with weaker results there (Fig. 4f) and the AM time series shows no significant association with the interannual variability of OLR over Southern Africa (Fig. 4g). The anticyclonic / cyclonic cells are however located quite similarly for all indices (Fig. 3). They mostly consist on an enhancement of the South Atlantic (Saint Helena) High and reduced poleward export of momentum over South America and Southern Africa during El Niño conditions. These features correspond well to the regional effects of ENSO over these sectors.

While ENSO's influence on the co-variability between the Southern American and South African regions at interannual timescale is dominant, other modes of climate variability could potentially be involved in the co-variability patterns previously identified. In addition to the results above, Figs. 4d-e and 4i-j present teleconnections between, on the one hand, global SST and regional OLR, and on the other hand, the AF and AM time series, after removing ENSO influence (shown in Figs. 4a,f). Results confirm the primary role of ENSO for both regions (Figs. 4a-c and 4f-h), but also suggest a secondary influence of:

(i) local / regional SST in the oceans adjacent to both regions (i.e. Southwest Atlantic for the American sector, subtropical Indian Ocean for Southern Africa). For the latter, the pattern

identified is reminiscent of the so-called “Subtropical Dipole” identified by Behera and Yamagata (2001), although its eastern pole off Australia is barely significant.

(ii) regional-scale anomalies in the OLR field. For the AM time series, they emerge over the Southern Atlantic and tropical Africa, which suggests that the interannual variability of the mid-latitude dynamics is partly decorrelated with ENSO, and directly influence southern South America. For the AF time series, similar conclusions are raised for large-scale atmospheric convection over the western Indian Ocean at tropical latitudes. This signal is not associated with clear SST variability (Fig. 4e) and should be interpreted with caution.

To sum up, co-variability in the large-scale convection between South America and Southern Africa at the interannual timescale is mostly, but not only, due to the common influence of ENSO. Consequently, associated patterns resemble more the regional ENSO effects over each sector than the CZ present over each region.

### *3.2 Intraseasonal timescale*

A CCA is here applied to daily OLR anomalies (after removal of the average annual cycle) computed over the same domains as Fig. 2. Prior to the analysis, input data were bandpass-filtered to retain the frequencies comprised between 25 and 75 days, with a 10-day lag period between the two regions (i.e., South America leads Southern Africa by 10 days). These filtering and lag parameters were set by a series of preliminary tests (not shown), which aimed at identifying robust and coherent modes of co-variability between the two regions.

The corresponding first mode of intraseasonal co-variability is shown in Fig. 5. It explains about 32% of the total intraseasonal co-variance between both domains. As for the interannual timescale (Section 3.1), these co-variability patterns are not clearly related to the SACZ and SICZ. The strongest signals are confined in the low latitudes (north of the Tropic of Capricorn), and are both weaker and noisier in the mid-latitudes. Associated time series show rather high correlation over the period ( $r = 0.51$ ), significant at the 99.99% confidence level considering their autocorrelation strongly reducing the degrees of freedom of both time series.

The frequencies at which the co-variability between the two regions is maximized are strongly reminiscent of the Madden-Julian Oscillation (MJO, Madden and Julian 1971; Madden and Julian 1972; Madden and Julian 1994; Zhang 2005), the leading mode of climate variability in the tropics

at the intraseasonal timescale. The MJO has already been shown to exert a significant influence over both regions (e.g., Carvalho et al. 2004 for South America ; Pohl et al. 2007 for Southern Africa). This is thus a potential candidate to explain the climate co-variability between both regions, even though this point has not been addressed *per se* in the literature so far. Two distinct supporting facts further reinforce the hypothesis of the MJO influence: (i) the MJO is a mode of tropical variability, modulating deep atmospheric convection mostly in the low latitudes, and its effects over both regions match well the spatial patterns shown in Fig. 5a (Carvalho et al. 2004; Pohl et al. 2007); (ii) the largest covariance between the two sectors is obtained for a lead-time of 10 days, matching once again the phase speed of the MJO: South America and Southern Africa being shifted by roughly  $90^\circ$  in longitude, it gives a period of about 40 days for the whole cycle – even though the MJO phase speed itself is not constant over all longitudes, see e.g. Salby and Hendon (1994); Bantzer and Wallace (1996); Matthews (2000).

Casarin and Kousky (1986) showed that a SACZ episode appears about 15 days after a SPCZ (Kuhnel 1989) episode, apparently through the propagation of the MJO. We aim here at clarifying this point for the two regions analyzed in this work (Figs. 5b-c). Fig. 5b first presents composite anomalies of the time series obtained from the CCA for the 8 phases of the MJO as defined by the RMM indices computed by WH04. The scores tend to be significantly negative (denoting enhanced convection in the tropical part of our domains) for phases 1-3 (during which the large-scale convection associated with the MJO initiate and develop over the western and central Indian Ocean) and positive (suppressed convection in tropical America and Africa) for phases 5 to 8 (suppressed convection over the Indian Ocean and enhanced convection over the Western Pacific and next weakening while propagating eastwards). It should be recalled that the signals appear perfectly in-phase between South America and Southern Africa, since the OLR time series were shifted by 10 days prior to the CCA. These results therefore do not suggest in-phase modulation of atmospheric convection by the MJO over the two regions.

Fig. 5c shows cross-spectral analyses between the same score time series and the RMM1 principal component. Similar results could be obtained using RMM2 instead, but with a phase relationship shifted by  $90^\circ$ . Results confirm significant associations between both CCA time series and RMM1 for periodicities comprised between roughly 15-20 days and  $>100$  days. At timescales from 30 to 60 days, the CCA time series share about 40% of their variance with RMM1. This confirms the predominant (but not exclusive) influence of the MJO on this mode of co-variability between the

two regions and quantifies the fraction of the time series variance that directly relates to the MJO. As for the interannual timescale, the co-variability between South America and Southern Africa (i) does not directly involve the SACZ and SICZ *stricto sensu*, (ii) mainly results from the influence of a mode of large-scale variability (here the MJO) affecting both regions. Further analysis of associated atmospheric dynamics and deep convective activity is given in Figs. 6, 7 and 8, respectively presenting the regional-scale circulation and OLR anomaly patterns associated with fluctuations in the AM and AF time series, together with composite anomalies based on RMM indices and describing the canonical signature of the MJO over the region. For the AM and AF analyses, the composites are constructed by extracting the extreme positive and negative phases ( $\pm 1$  standard deviation) of the time series shown in Fig. 5, and next plotting the synchronous and lagged differences in OLR and wind anomalies. The lags introduced, spanning between -25 and +25 days, are chosen to document roughly the life cycle of an MJO event. Over South America, episodes of enhanced convection (between Day 0 and Day +20, Fig. 6) are concomitant with a transient enhancement of the South Atlantic High throughout the troposphere; over the Amazonia basin it is also associated with lower-layer northwesterly anomalies. These patterns are roughly opposite to those associated with the suppressed convection prevailing between Day -15 and Day 0, i.e. before the peaks in the AM time series of Fig. 5. They are consistent with the intraseasonal anomalies found to recurrently modulate large-scale convection over the region in Carvalho et al. (2002a; 2002b). Also interesting is the fact that, between Day +5 and Day +15 (i.e. a few days after the development of convection in South America), negative OLR (active convection) and lower-layer northwesterly anomalies similarly develop over the Southern African sector. Dry anomalies symmetrically develop there between Day -15 and Day 0, lagging once again the positive OLR anomalies over South America. The wet episodes over South America are reminiscent of the anomalies associated with MJO phases 8 and 1 (Fig. 8), i.e. those associated with enhanced convection over the western Hemisphere and Africa (WH04, their Fig. 7). It is worth noting that, in agreement with previous studies, atmospheric dynamics associated with the MJO extends in the mid-latitudes (Matthews and Meredith 2004; Pohl et al. 2010) and even high southern latitudes (Flatau and Kim 2013; Fauchereau et al. 2016), even if associated convective anomalies are confined to the tropics and involve no clear continuities with the extra-tropics (Figs. 5a, 6-7-8). Moreover, the similarity between the “canonical” MJO signature over the region and the wet / dry phases over South America is not perfect, which suggests that the MJO

drives only part of the regional convective intraseasonal variability (40% according to Fig. 5b, indicating that other phenomena independent from the MJO are involved in the intraseasonal variability and co-variability such as extracted here). A potential candidate is the South Atlantic High, which shows variability only partly related to the MJO, and influences mass flux convergence over tropical South America. Indeed, the anomaly patterns shown in Fig. 6 match very well those found in Carvalho et al. (2004) to correspond to “intense” and “weak” SACZ events (referred to as wet and dry phases in this study, respectively), hereby suggesting a non-negligible intrinsic variability that develops at the local / regional scales. Numerical ensemble experiments performed e.g. with a regional climate model used in the CLARIS / South America CORDEX framework (Solman 2013) should allow disentangling the large-scale versus regional-scale fractions of convective variability in this region.

For Southern Africa (Fig. 7), enhanced convection (Day0 to Day +20) is associated with lower-layer easterly anomalies favoring moisture advections from the Indian Ocean towards Africa. They first develop over the west coast of Southern Africa before migrating eastwards and next northwards. This corresponds to the signature of the MJO there (Fig. 8, phases 6 to 1). Opposite-sign patterns prevailing between Day -15 and Day 0 (Fig. 7) are similarly close to the MJO phases 2 to 5, associated with dry anomalies (Fig. 8). In agreement with Fig. 6, largest convective anomalies (of both signs) tend to develop over Southern Africa a few days after their largest intensities over South America. The symmetry between the two regions is thus rather evident, albeit not perfect. For both regions, the influence of the MJO is thus predominant, but more regional phenomena and mechanisms influence both regions separately and act to decouple their variability at the intraseasonal timescale. As for the South American sector, Southern African convective anomalies at the intraseasonal timescale are associated with temperate anomalies over the South Atlantic, but also circulation anomalies over the Indian Ocean, both influencing large-scale convergence over the region. Due to such interferences with regional-scale climate variability, both AF and AM series share only 30-40% of their total variance, at intraseasonal timescales, with the global-scale MJO (Fig. 5c).

In short, the main result in this section is similar to the interannual timescale: a significant but partial influence of a mode of large-scale variability, namely the MJO, is here responsible for convective co-variability between the two regions at the intraseasonal timescale. In the mid-latitudes, variability of the South Atlantic High associated with the MJO appears as a key

circulation pattern modulating mass flux convergence and thus convective activity over both regions.

### *3.3 Synoptic scale*

This section corresponds to the most novel contribution of the present study. As for the intraseasonal timescale, a series of preliminary analyses were conducted using various band-pass filters and lags in order to find the modes maximizing the co-variance between the two regions. However, unlike previous timescales, for which the most appropriate choice was quite evident, two robust modes of co-variability emerged when filtering input OLR data so that synoptic variability is retained (that is, using a 10-day highpass filter). The most robust mode is found for synchronous co-variability between South America and Southern Africa (i.e. in-phase convective fluctuations in both regions). A second, slightly weaker mode is found for a lag of 4 days (South America leads Southern Africa); this mode has been recently identified and discussed by Grimm and Reason (2015).

For conciseness, only the first mode is analyzed in details here (Fig. 9), and we will only discuss briefly the second one. Contrary to results presented for the interannual and intraseasonal timescales, the regions showing significant co-variability at the synoptic timescale match well the typical spatial signature of both CZ (i.e., the SACZ in South America and the SICZ in Southern Africa, see the Introduction). It is also worth noting that these spatial patterns correspond well to the dominant modes of large-scale convective synoptic variability when extracted over each region separately (see the Appendix). Convective signals co-vary in phase between the two sectors, but share a sensibly lower fraction of variance compared to the intraseasonal timescale ( $R = 0.25$ ). This is due to the larger number of DOF (Fig. 9) and the noisier character of associated time series. Yet, the latter are still correlated at a 99.99% significance level (even when considering their serial autocorrelation). Over the American domain, the largest co-variance is found over the oceanic part of the region, that is the Southern Atlantic, along a northwest-southeast oriented band clearly reminiscent of the SACZ structure. That is, the oceanic part of the domain exhibits largest co-variance with African convection than the continental part. Over Southern Africa, similar alignments prevail, which are also in good agreement with the spatial signature of the SICZ (or



TTT systems when synoptic time-scales are exclusively considered). There, land-sea contrasts are of weaker importance.

Associated atmospheric dynamics and convection are shown in Figs. 10 and 11. They are obtained as lagged composite analyses between the opposite phases of the AM and AF series shown in Fig. 9, respectively. Episodes of enhanced convection over South America are embedded in a wave train well discernible two days before the convective burst. Associated wind and convective anomalies develop and peak at Day 0 (synchronously with the local maxima of the AM time series) and gradually elongate from northwest to southeast before weakening (Day +2 to +4) and dissipating (Day +6). This structure, already described in *e.g.* Van der Wiel et al. (2015), is clearly reminiscent of an atmospheric Rossby wave triggering convection through baroclinic instability. The same pattern and the same mechanisms are found over the Southern African sector. The development, peak and decay of vorticity anomalies are synchronous between both regions (with largest wave amplitudes found between Day -2 and Day +2).

Comparing Figs. 10 and 11 reveals that each sector is influenced by an atmospheric Rossby wave modulating its atmospheric convection, but with no clear association with the remote region –in other words, anomalies are weak, on average, over Southern Africa during AM events, and South America during AF events. This may seem as counter-intuitive, since the time series extracted from the CCA (Fig. 9) are associated with a mode designed to maximize co-variability between the two regions. This is due to the intermittency of the co-variability between the AF and AM regions (Table 1). Only  $\frac{1}{4}$  of the convective bursts in the AM domain (143 days out of 608) are associated with a synchronous burst in the AF region, and the same fraction is also verified for the clear-sky conditions in both regions (165 days out of 612). This intermittency contributes to explain the relative weakness of the positive correlation between both time series (Fig. 9). Yet, Table 1 confirms that they clearly tend to co-vary in phase. Very few days are characterized by synchronous out-of-phase convective anomalies between the two sectors (59 show active convection in AM and suppressed convection in AF, and 49 the other way around).

Fig. 12 shows the composite analyses of atmospheric dynamics and convection during the joined and synchronous phases of both AM and AF time series. The resulting pattern roughly corresponds to the union of those shown in Figs. 10 and 11, i.e., they combine the vorticity over both sectors through a continuous wave train over the whole South Atlantic, linking both CZ, and modulating large-scale atmospheric convection over both sectors. Although it is too rare to appear on average

when working on each sector specifically, this continuous wave train is shown here (Table 1, Fig. 12) to contribute to about 25% of the active AM and AF events and is thus non-negligible to explain their overall temporal variability. These results are consistent and complement those obtained by idealized numerical experiments by Cook et al. (2004)

To sum up, synchronous convective bursts between both regions at short timescales are due to the development of a wave train in the mid-latitudes. This is an intermittent phenomenon, which occurs on average during only one quarter of the convective burst of each region, the remaining ones showing no concomitant anomalies over the remote region. The same conclusions hold for opposite sign anomalies, that is, synchronous clear sky conditions developed over both sectors. The predominance, for the synoptic scale, of this “synchronous” mode of variability (Fig. 9) against a weaker (yet significant) mode with a 4-day-lag between the two regions (Grimm and Reason 2015), suggests that the development of the wave train over the South Atlantic is more frequent and accounts for a larger part of the co-variability between the two regions, than other mechanisms involving wave propagations over the sector (such as a baroclinic instability developing over the AM region, next propagating eastwards and finally modulating atmospheric convection a few days later over Southern Africa). Such phenomena are nevertheless thought to have a physical reality, even though it is of weaker importance for both regions. It is thus not discussed in details in the present study.

### *3.4 Scale interactions*

Fig. 13 finally presents results illustrating the scale interactions between the various timescales and regions analyzed and discussed in the previous sections.

ENSO has already been shown to interact with intraseasonal (Pohl and Matthews 2007) and synoptic-scale (Carvalho et al. 2004; Fauchereau et al. 2009; Pohl et al. 2009) variability over both regions. More precisely, ENSO tends to favor (i) higher-frequency (i.e. shorter) MJO events (Pohl and Matthews 2007); (ii) spatial shifts in the location of both CZ, which translates into interannual modulations of the synoptic-scale convective bursts over both continents. Figs. 13a-d indicates to what extent ENSO modulates the seasonal variance of the high-frequency modes of co-variability shown in Figs. 5 and 9.

None of the scale interactions involving ENSO is statistically significant (at the 95% level). One can only conclude that intraseasonal convective variability tends to be larger over both regions during El Niño conditions, a result already suggested by Pohl et al. (2007) over Southern Africa. The strongest relationship identified here concerns synoptic-scale variability over South America, also found to be stronger than normal during El Niño (Fig. 13a). There is no equivalent for Southern Africa: while ENSO modulates the “continental” (i.e. westernmost) TTTs embedded in the SICZ, it seems to impact their only location (i.e. during El Niño, TTT are shifted eastward) rather than their overall frequency.

Relationships between intraseasonal (MJO) and synoptic-scale variabilities are next assessed through cross-spectral analyses (Figs. 13e-h). Pohl et al. (2009) previously concluded on the lack of clear and significant scale interactions at these time-scales over Southern Africa. More recently, Oettli et al. (2014) and Hart et al. (2013) suggested possible (but weak) relationships, consisting in a modulation by the MJO of the intensities (but not their location nor their frequency) of TTTs over Southern Africa. The analyses carried in this work tend to support the conclusions of Pohl et al (2009) and do to show any significant relationships between these timescales (Figs. 13g-h). Note however that the methodologies used here are not able to capture explicitly the intensity of synoptic systems such as TTTs.

Figs. 13e-f finally document the relationships between the two regions, based on the “intraseasonal” and “synoptic” time series (resp. shown in Figs. 5 and 9). Confirming previous results, the two time series show up to 50% of common variance at the typical frequencies of the MJO (Fig. 13e). As stated above, even though they are influenced by a common mode of large-scale variability, both regions nonetheless show some non-negligible intrinsic variability. The latter should however not be overestimated, the MJO being “active” only about 50% of the time (WH04). The common variance is weaker for the synoptic scale (Fig. 13f), peaking at most at 30%. This is presumably due to the intermittent nature of the co-variability between the two sectors at this timescale (Table 1). Yet, statistical associations between the two regions are significant for frequencies higher than 10 days, a logical result given the settings of the filter used for this timescale.

#### **4. Conclusion and discussion**

561

562 This study aimed at characterizing patterns of co-variability between South American and  
563 Southern African large-scale atmospheric convection at various timescales (ranging from synoptic  
564 to interannual), and identifying associated mechanisms and processes. The main results can be  
565 summarized as follows:

566 (i) At the interannual timescale, both regions are influenced by ENSO and tend to co-vary in phase.  
567 Both tropical Africa (including Equatorial East Africa) and southeastern Brazil / northern  
568 Argentina tend to experience wetter than normal conditions during El Niño. Southern Africa and  
569 northern Brazil tend to record opposite anomalies. The influence of ENSO in Southern Africa  
570 being complex and not systematic (Reason and Jagadheesha 2005), the co-variability pattern  
571 identified in this work is not significant over that area. This indicates that ENSO influence,  
572 although strong and highly significant, interferes with other phenomena / modes of variability at  
573 this timescale, including e.g. the Subtropical Dipole over the Indian Ocean (Behera and Yamagata  
574 2001) or more local variability patterns in the Southern Atlantic or Indian basins. 60% of the  
575 interannual variability in each American and African region linearly relates to the state of ENSO  
576 and these two regions share also about the same percentage of variance.

577 (ii) At the intraseasonal timescale, both regions are once again placed under the common (but  
578 partial) influence of a mode of large-scale climate variability, namely, the MJO. Large-scale  
579 convective anomalies over South America, either positive or negative, lead those of Southern  
580 Africa by 10 days (i.e. roughly  $\frac{1}{4}$  of the typical MJO life cycle). At the typical frequency bin of  
581 the MJO (30-60 days), both regions show about 35-40% of common variance with a global-scale  
582 MJO descriptor, and share about 50% common variance. In both areas, deep convective anomalies  
583 solely concern the tropical part of the domain, the temperate latitudes showing nonetheless strong  
584 dynamical signals consisting mostly in an intraseasonal modulation of the South Atlantic High.  
585 The latter seem to be particularly relevant to influence mass flux convergence over both sectors,  
586 and thus large-scale convective variability. Part of its variability is related to the MJO (hereby  
587 confirming previous work, e.g. Matthews and Meredith 2004), but such circulation anomalies also  
588 account for a (limited) fraction of extra co-variability.

589 (iii) At the synoptic scale co-variability is weaker and the time series associated with each region  
590 are much noisier. They show only 6% of common variance. The spatial patterns however  
591 correspond well to the spatial signatures of the SACZ and SICZ. Importantly, convective

anomalies tend to occur synchronously in the two sectors, i.e., in-phase enhanced or suppressed convection occur in both CZ. Physically, large-scale convective activity in each region is triggered by atmospheric Rossby waves in the mid-latitudes. In-phase convection between the two regions occurs only 25% of the time, the remaining 75% corresponding to a transient enhancement or suppression of convection over one sector without any significant changes over the remote region. When both regions show in-phase anomalies, it is associated with a continuous wave train developing over the Southern Atlantic and linking America and Africa. In the other cases, the wave train is interrupted between the two longitudes, over the Atlantic Ocean, and atmospheric convection is thus significantly modified over one single continent. In the end, at timescales longer than  $\sim 10$  days, South American and Southern African convection can show up to 20-30% of common variance, a magnitude intuitively coherent with the fact that  $\frac{1}{4}$  of the Rossby waves triggering convection over one given region is accompanied by another one located at the same time over the second sector. Our results also suggest that another mode of co-variability relates both regions at this timescale, and consists in deep convective anomalies developing first over the American region and next, four days later, over Africa. This mode, which could be interpreted as the propagation of a Rossby wave over the Southern Atlantic, seems however to be weaker and less robust than the synchronous mode detailed and presented in this work. It is also thought to account for a more limited amount of common variance between South America and Southern Africa.

(iv) Finally, scale interactions between the aforementioned scales and phenomena are investigated. Results suggest possible (but barely significant) intensification of intraseasonal variability over both South America and Southern Africa during El Niño events. Possible modulation of synoptic-scale variability by ENSO is also suggested over the American region only. No significant relationship is found between the intraseasonal and synoptic scales, i.e. the occurrences or co-occurrences of Rossby wave(s) over our two domains do not seem to be strongly modulated by the phase of the MJO within the tropics.

Our results contribute to a better understanding of the factors that influence regional-scale convective fluctuations in the South American and Southern African sectors. They also provide a clearer picture of the co-occurrences of cloud bands over the Southern Hemisphere, clearly visible over satellite images of the Southern Hemisphere, and about which little is known. In future work, transposing such analyses to the third convergence zone of the Southern Hemisphere, namely the

South Pacific Convergence Zone (SPCZ), could complete the picture of the variabilities and co-variabilities affecting and modulating the intensity, extension and location of these zones.

## **Appendix. Dominant modes of large-scale convective variability in each region**

The Canonical Correlation Analyses used in this work aim at maximizing the co-variability between two domains. The modes extracted could possibly differ from the leading modes of variability calculated for each region separately. This case would imply that the mode extracted probably accounts for a reduced fraction of the regional climate variability in each region and could thus correspond more to a statistical artifact than a physically robust mechanism.

Figs. S1 and S2 present therefore the leading EOF of PCA applied to raw (unfiltered) OLR anomalies in each region. Both analyses extract the robust variability patterns, already presented in many previous papers for both regions (e.g., Carvalho et al. 2004; Pohl et al. 2009), which are associated with the spatio-temporal variability of both CZ. These patterns sensibly differ from those found at the interannual (Fig. 2) and intraseasonal (Fig. 5) timescales, which are discussed in this study. The latter are however in fair agreement with the spatial signature of ENSO and the MJO over these sectors, respectively, which confirms the hypothesis of significant co-variabilities caused by the common influence of a single, larger-scale atmospheric or climatic phenomenon encompassing both regions.

The spatial similarity is largest for the synoptic scale, counter-balancing a weaker and intermittent temporal co-variability. For this timescale, one can thus conclude that the mode of co-variability shown in Fig. 9 corresponds to the leading variability patterns influencing each region. Unlike the longer timescales, one can here conclude on co-variability between the “SACZ” and “SICZ”, strictly speaking, and not merely on the South American and Southern African regions.

## **Acknowledgments**

This study is dedicated to the memory of Professor Gérard Beltrando. The authors thank Dr. Josyane Ronchail for helpful comments that helped improve the manuscript, and two anonymous reviewers for their suggestions that helped improve the manuscript. ERA-Interim data were

655 provided by ECMWF. N. Fauchereau acknowledges funding provided by the NIWA project  
656 “Climate Present and Past” CAO1601 within the Climate Observations Programme in the  
657 National Climate Centre. Calculations were performed using HPC resources from DSI-CCuB  
658 (université de Bourgogne).

659

## References

- Bantzer CH, Wallace JM (1996) Intraseasonal variability in tropical mean temperature and precipitation and their relation to the tropical 40-50 day oscillation. *J Atmos Sci* 53:3032–3045. doi: 10.1175/1520-0469(1996)053<3032:IVITMT>2.0.CO;2
- Barreiro M, Chang P, Saravanan R (2002) Variability of the South Atlantic convergence zone simulated by an atmospheric general circulation model. *J Clim* 15:745–763. doi: 10.1175/1520-0442(2002)015<0745:VOTSAC>2.0.CO;2
- Behera SK, Yamagata T (2001) Subtropical SST dipole events in the southern Indian Ocean. *Geophys Res Lett* 28:327–330. doi: 10.1029/2000GL011451
- Boulard D, Pohl B, Crétat J, et al. (2013) Downscaling large-scale climate variability using a regional climate model: the case of ENSO over Southern Africa. *Clim Dyn* 40:1141–1168. doi: 10.1007/s00382-012-1400-6
- Carvalho LM V, Jones C, Liebmann B (2004) The South Atlantic Convergence Zone: Intensity, Form, Persistence, and Relationships with Intraseasonal to Interannual Activity and Extreme Rainfall. *J Clim* 17:88–108.
- Carvalho LM V, Jones C, Liebmann B (2002a) Extreme Precipitation Events in Southeastern South America and Large-Scale Convective Patterns in the South Atlantic Convergence Zone. *J Clim* 15:2377–2394.
- Carvalho LM V, Jones C, Silva Dias MAF (2002b) Intraseasonal large-scale circulations and mesoscale convective activity in tropical South America during the TRMM-LBA campaign. *J Geophys Res* 107:D20. doi: 10.1029/2001JD000745
- Carvalho LM V, Silva AE, Jones C, et al. (2011) Moisture transport and intraseasonal variability in the South America monsoon system. *Clim Dyn* 36:1865–1880. doi: 10.1007/s00382-010-0806-2
- Casarin DP, Kousky VE (1986) Anomalias de Precipitação No Sul Do Brasil E Variações Na Circulação Atmosférica. *Rev Bras Meteorol* 1:83–90.
- Cazes-Boezio G, Robertson AW, Mechoso CR (2003) Seasonal dependence of ENSO teleconnections over South America and relationships with precipitation in Uruguay. *J Clim* 16:1159–1176. doi: 10.1175/1520-0442(2003)16<1159:SDOETO>2.0.CO;2
- Cook KH (2003) Reply to “Comments on ”The South Indian Convergence Zone and interannual rainfall variability over Southern Africa“ and the question of ENSO’s influence on Southern Africa.” *J Clim* 16:563–565.
- Cook KH (2000) The South Indian Convergence Zone and Interannual Rainfall Variability over Southern Africa. *J Clim* 13:3789–3804.
- Cook KH (2001) A Southern Hemisphere Wave Response to ENSO with Implications for Southern Africa Precipitation. *J Atmos Sci* 58:2146–2162. doi: 10.1175/1520-0469(2001)058<2146:ASHWRT>2.0.CO;2
- Cook KH, Hsieh JS, Hagos SM (2004) The Africa-South America intercontinental teleconnection. *J Clim* 17:2851–2865. doi: 10.1175/1520-0442(2004)017<2851:TAAIT>2.0.CO;2
- Dee DP, Uppala SM, Simmons AJ, et al. (2011) The ERA-Interim reanalysis : configuration and performance of the data assimilation system. *Q J R Meteorol Soc* 137:553–597. doi: 10.1002/qj.828
- Fauchereau N, Pohl B, Lorrey A (2016) Extratropical Impacts of the Madden–Julian Oscillation over



702 New Zealand from a Weather Regime Perspective. *J Clim* 29:2161–2175. doi: 10.1175/JCLI-D-15-  
703 0152.1

704 Fauchereau N, Pohl B, Reason CJC, et al. (2009) Recurrent daily OLR patterns in the Southern  
705 Africa/Southwest Indian Ocean region, implications for South African rainfall and teleconnections.  
706 *Clim Dyn* 32:575–591. doi: 10.1007/s00382-008-0426-2

707 Figueroa SN, Satyamurty P, Silva Dias PL (1995) Simulations of the summer circulation over the South  
708 American region with an eta coordinate model. *J Atmos Sci* 52:1573–1584.

709 Flatau M, Kim Y-J (2013) Interaction between the MJO and Polar Circulations. *J Clim* 26:3562–3574.  
710 doi: 10.1175/JCLI-D-11-00508.1

711 Grimm A, Reason CJC (2015) Intraseasonal teleconnections between South America and southern Africa.  
712 *J Clim* 28:9489–9497. doi: 10.1175/JCLI-D-15-0116.1

713 Grimm AM, Barros VR, Doyle ME (2000) Climate Variability in Southern South America Associated  
714 with El Niño and La Niña Events. *J Clim* 13:35–58. doi: 10.1175/1520-  
715 0442(2000)013<0035:CVISSA>2.0.CO;2

716 Hart NCG, Reason CJC, Fauchereau N (2013) Cloud bands over southern Africa: seasonality,  
717 contribution to rainfall variability and modulation by the MJO. *Clim Dyn* 41:1199–1212. doi:  
718 10.1007/s00382-012-1589-4

719 Jorgetti T, da Silva Dias PL, de Freitas ED, et al. (2014) The relationship between South Atlantic SST  
720 and SACZ intensity and positioning. *Clim Dyn* 42:3077–3086. doi: 10.1007/s00382-013-1998-z

721 Jury MR (2002) Economic Impacts of Climate Variability in South Africa and Development of Resource  
722 Prediction Models. *J Appl Meteorol* 41:46–55. doi: 10.1175/1520-  
723 0450(2002)041<0046:EIOCVI>2.0.CO;2

724 Kalnay E, Kanamitsu M, Kistler R, et al. (1996) The NCEP/NCAR 40-Year Reanalysis Project. *Bull Am*  
725 *Meteorol Soc* 77:437–471.

726 Kodama YM (1992) Large-Scale Common Features of Subtropical Precipitation Zones (the Baiu Frontal  
727 Zone, the SPCZ, and the SACZ). Part I: Characteristics of Subtropical Frontal Zones. *J Meteorol*  
728 *Soc Japan* 70:813–836.

729 Kodama YM (1993) Large-scale common features of subtropical convergence zones (the Baiu frontal  
730 zone, the SPCZ, and the SACZ). Part II: Conditions of the circulations for generating the STCZs. *J*  
731 *Meteorol Soc Japan* 71:581–610.

732 Krishnamurthy V, Misra V (2010) Observed ENSO teleconnections with the South American monsoon  
733 system. *Atmos Sci Lett* 11:7–12. doi: 10.1002/asl.245

734 Kuhnel I (1989) Tropical-Extratropical Cloudband Climatology Based on Satellite Data. *Int J Climatol*  
735 9:441–463.

736 Lenters JD, Cook KH, Ringler TD (1995) Comments on “On the influence of the Andes on the general  
737 circulation of the Southern Hemisphere.” *J Clim* 8:2113–2115.

738 Liebmann B, Kiladis GN, Marengo JA, et al. (1999) Submonthly Convective Variability over South  
739 America and the South Atlantic Convergence Zone. *J Clim* 12:1877–1891.

740 Liebmann B, Smith CA (1996) Description of a complete (interpolated) outgoing longwave radiation  
741 dataset. *Bull Am Meteorol Soc* 77:1275–1277.

742 Lyon B, Mason SJ (2007) The 1997–98 Summer Rainfall Season in Southern Africa. Part I:

743 Observations. *J Clim* 20:5134–5148. doi: 10.1175/JCLI4225.1

744 Lyon B, Mason SJ (2009) The 1997/98 Summer Rainfall Season in Southern Africa. Part II: Model  
745 Simulations and Coupled Model Forecasts. *J Clim* 22:3802–3818. doi: 10.1175/2009JCLI2600.1

746 Macron C, Pohl B, Richard Y, Bessafi M (2014) How do Tropical Temperate Troughs Form and Develop  
747 over Southern Africa? *J Clim* 27:1633–1647. doi: 10.1175/JCLI-D-13-00175.1

748 Madden RA, Julian PR (1971) Detection of a 40-50 Day Oscillation in the Zonal Wind in the Tropical  
749 Pacific. *J Atmos Sci* 28:702–708.

750 Madden RA, Julian PR (1972) Description of Global-Scale Circulation Cells in the Tropics with a 40-50  
751 Day Period. *J Atmos Sci* 29:1109–1123.

752 Madden RA, Julian PR (1994) Observations of the 40-50-day tropical oscillation - A Review. *Mon*  
753 *Weather Rev* 122:814–837.

754 Mason SJ, Jury MR (1997) Climatic variability and change over southern Africa: a reflection on  
755 underlying processes. *Prog Phys Geogr* 21:23–50. doi: 10.1177/030913339702100103

756 Matthews AJ (2000) Propagation Mechanism for the Madden-Julian Oscillation. *Q J R Meteorol Soc*  
757 126:2637–2652.

758 Matthews AJ, Meredith MP (2004) Variability of Antarctic circumpolar transport and the Southern  
759 Annular Mode associated with the Madden-Julian Oscillation. *Geophys Res Lett* 31:L24312. doi:  
760 10.1029/2004GL021666

761 Der Mégréditchian G (1992) Le traitement statistique des données multi-dimensionnelles: application à la  
762 météorologie. *Cours manuels l'ENM Vol. 8.* p 287

763 Misra V (2003) The Influence of Pacific SST Variability on the Precipitation over Southern Africa. *J*  
764 *Clim* 16:2408–2418.

765 Nicholson SE (2015) Long-term variability of the East African “short rains” and its links to large-scale  
766 factors. *Int J Climatol.* doi: 10.1002/joc.4259

767 Nicholson SE (1997) An analysis of the ENSO signal in the tropical Atlantic and western Indian oceans.  
768 *Int J Climatol* 17:345–375.

769 Nicholson SE, Kim J (1997) The relationship of the El Niño-Southern Oscillation to African rainfall. *Int.*  
770 *J. Climatol.* 17:

771 Oettli P, Tozuka T, Izumo T, et al. (2014) The self-organizing map, a new approach to apprehend the  
772 Madden–Julian Oscillation influence on the intraseasonal variability of rainfall in the southern  
773 African region. *Clim Dyn* 43:1557–1573. doi: 10.1007/s00382-013-1985-4

774 Pohl B, Fauchereau N, Reason CJC, Rouault M (2010) Relationships between the Antarctic Oscillation,  
775 the Madden–Julian Oscillation, and ENSO, and Consequences for Rainfall Analysis. *J Clim* 23:238–  
776 254. doi: 10.1175/2009JCLI2443.1

777 Pohl B, Fauchereau N, Richard Y, et al. (2009) Interactions between synoptic, intraseasonal and  
778 interannual convective variability over Southern Africa. *Clim Dyn* 33:1033–1050. doi:  
779 10.1007/s00382-008-0485-4

780 Pohl B, Matthews AJ (2007) Observed Changes in the Lifetime and Amplitude of the Madden–Julian  
781 Oscillation Associated with Interannual ENSO Sea Surface Temperature Anomalies. *J Clim*  
782 20:2659–2674. doi: 10.1175/JCLI4230.1

783 Pohl B, Richard Y, Fauchereau N (2007) Influence of the Madden–Julian Oscillation on Southern African

784 Summer Rainfall. *J Clim* 20:4227–4242. doi: 10.1175/JCLI4231.1

785 Rayner NA, Brohan P, Parker DE, et al. (2006) Improved Analyses of Changes and Uncertainties in Sea  
786 Surface Temperature Measured In Situ since the Mid-Nineteenth Century: The HadSST2 Dataset. *J*  
787 *Clim* 19:446–469.

788 Reason CJC, Jagadheesha D (2005) A model investigation of recent ENSO impacts over southern Africa.  
789 *Meteorol Atmos Phys* 89:181–205. doi: 10.1007/s00703-005-0128-9

790 Robertson AW, Mechoso C (2000) Interannual and decadal variability of the South Atlantic convergence  
791 zone. *Mon Weather Rev* 128:2947–2957.

792 Salby ML, Hendon HH (1994) Intraseasonal behavior of clouds, temperature, and motion in the tropics. *J*  
793 *Atmos Sci* 51:2207–2224. doi: 10.1175/1520-0469(1994)051<2207:IBOCTA>2.0.CO;2

794 Simmons AJ, Uppala SM, Dee DP, Kobayashi S (2007) ERA-interim: new ECMWF reanalysis products  
795 from 1989 onwards. *ECMWF Newsl* 110:25–35.

796 Solman SA (2013) Regional Climate Modeling over South America : A Review. *Adv Meteorol*  
797 2013:504357. doi: 10.1155/2013/504357

798 Streten NA (1973) Some Characteristics of Satellite-Observed Bands Of Persistent Cloudiness Over the  
799 Southern Hemisphere. *Mon Weather Rev* 101:486–495. doi: 10.1175/1520-  
800 0493(1973)101<0486:SCOSBO>2.3.CO;2

801 Todd M, Washington R (1999) Circulation anomalies associated with tropical-temperate troughs in  
802 southern Africa and the south west Indian Ocean. *Clim Dyn* 15:937–951. doi:  
803 10.1007/s003820050323

804 Todd MC, Washington R (1998) Extreme daily rainfall in southern Africa and southwest Indian Ocean:  
805 Tropical–temperate links. *S Afr J Sci* 94:64–70.

806 Vigaud N, Pohl B, Crétat J (2012) Tropical-temperate interactions over southern Africa simulated by a  
807 regional climate model. *Clim Dyn* 39:2895–2916. doi: 10.1007/s00382-012-1314-3

808 Vincent DG (1994) The South Pacific Convergence Zone (SPCZ): A Review. *Mon Weather Rev*  
809 122:1949–1970.

810 Wheeler MC, Hendon HH (2004) An All-Season Real-Time Multivariate MJO Index : Development of an  
811 Index for Monitoring and Prediction. *Mon Weather Rev* 132:1917–1932.

812 Widlansky MJ, Webster PJ, Hoyos CD (2011) On the location and orientation of the South Pacific  
813 Convergence Zone. *Clim Dyn* 36:561–578. doi: 10.1007/s00382-010-0871-6

814 Van Der Wiel K, Matthews AJ, Stevens P, Joshi MM (2015) A dynamical framework for the origin of the  
815 diagonal South Pacific and South Atlantic Convergence Zones. *Q J R Meteorol Soc* 141:1997–2010.  
816 doi: 10.1002/qj.2508

817 Wolter K, Timlin MS (1993) Monitoring ENSO in COADS with a seasonally adjusted principal  
818 component index. In: Norman OK (ed) 17th Clim. Diagnostics Work. pp 52–57

819 Zhang C (2005) Madden-Julian Oscillation. *Rev Geophys* 43:RG2003. doi: 10.1029/2004RG000158

820

## Figure Captions

**Figure 1** Study domain for the "South American" sector (in blue: 50°S-0°, 70°W-10°W) and "Southern African" sector (in red: 40°S-10°S, 7.5°E-70°E), as well as the large region encompassing both domains. Shadings represent the austral summer (November through February) seasonal mean OLR field ( $\text{W m}^{-2}$ ).

**Figure 2** Canonical correlation analysis of seasonal mean OLR co-variability at the interannual timescale between the "South American" and "Southern African" sectors, period NDJF 1979-2012. Upper panels: first mode of co-variability, displayed through heterogeneous correlation maps. Dashed curves show the 95% significance bound according to a Bravais-Pearson test. The squared coherence fraction (SCF) is labeled in the figure. Lower panel: associated time series, represented together with the seasonal mean Multivariate ENSO Index (MEI, multiplied by -1 for readability) over the same period. The correlation matrix between these time series and their actual number of degrees of freedom (considering possible serial auto-correlation) are indicated in the figure.

**Figure 3** Interannual correlations between the seasonal mean and horizontal wind at 200hPa (left-hand panels) and 850hPa (right-hand panels), and the three time series shown in Fig. 2. Only 95% significant correlations according to a Bravais-Pearson test are displayed.

**Figure 4** (a) Interannual correlations between the seasonal mean SST and synchronous MEI, period NDJF 1979-2012. Black contours show 95% significant correlations according to a Bravais-Pearson test. (b, c) As (a) but for the AM and AF time series of Fig. 2, respectively. (d, e) As (b,c) but after removing linearly the influence of the synchronous MEI. (f-j) As (a-e) but correlations with the seasonal mean OLR field over the domain shown in Fig. 1.

**Figure 5** (a) Canonical correlation analysis of 25-75-day bandpass filtered (intraseasonal) OLR co-variability between the "South American" and "Southern African" sectors, period NDJF 1979-2012. Upper panels: as Fig. 2, upper panels. A lag of 10 days is here applied between the two regions (South America leads Southern Africa by 10 days). Central panel: associated time series, their correlation and actual number of degrees of freedom. (b) Composite analysis of the CCA time series for the 8 phases of the MJO as defined by the RMM indices. Only days characterized by an MJO amplitude larger than one standard deviation are considered. Asterisks denote 95% significant anomalies according to a *t*-test. (c) Cross-spectral analysis between the CCA time series and RMM1 index. All analyses are carried out on normalized data for the NDJF 1979-2012 period, with other months padded with zeros. Thick lines: squared coherence. Dashed lines: 95% level according to 1000 random time series obtained as permutations of the original time series, and having the same lag-1 serial correlation. Thin lines: phase relationship in degrees.

**Figure 6** Lead-lag composite analysis of daily OLR (shadings,  $\text{W m}^{-2}$ ), horizontal wind (vectors,  $\text{m s}^{-1}$ ) at 200hPa (left-hand panels) and 850hPa (right-hand panels), and opposite phases ( $>1$  standard deviation minus  $<-1$  standard deviation) of the AM time series shown in Fig. 5. Only 95% significant differences according to a two-tailed  $t$ -test (for OLR) and  $t^2$ -test (for the wind) are displayed. The  $t^2$ -test, also known as Hotelling test, is the multivariate generalization of the  $t$ -test.

**Figure 7** As Fig. 6 but based on the AF time series of Fig. 5.

**Figure 8** Composite analysis of OLR (shadings,  $\text{W m}^{-2}$ ), horizontal wind (vectors,  $\text{m s}^{-1}$ ) at 200hPa (a) and 850hPa (b) for the 8 phases of the MJO as defined by the RMM indices. Significance is tested as for Fig. 6. Only days characterized by an MJO amplitude larger than one standard deviation are considered in the analysis.

**Figure 9** As Fig. 5a but for 10-day highpass filtered (synoptic-scale) OLR. No lag (synchronous OLR fields) is applied between the two regions.

**Figure 10** As Fig. 6 but based on the AM time series of Fig. 9.

**Figure 11** As Fig. 6 but based on the AF time series of Fig. 9.

**Figure 12** As Fig. 6 but extracting the synchronous opposite phases of both AM and AF time series of Fig. 9 (i.e., “both positive” minus “both negative” events).

**Figure 13** Scale interactions between the interannual, intraseasonal and synoptic modes of variability and co-variability. (a) Interannual vs. synoptic in the AM region. Box-and-whisker representation of the seasonal variance of the AM time series for the synoptic scale, during El Niño, neutral ENSO and La Niña years. The boxes have lines at the lower quartile, median and upper quartile values. The whiskers are lines extending from each end of the box to show the range of the data. Outliers (outside of 1.5 inter-quartile range) appear as plus signs. (b) As (a) for the AF domain. (c, d) As (a,b) but for interannual vs. intraseasonal timescales. (e) AF vs. AM, intraseasonal scale. Cross-spectral analysis between the two time series of Fig. 6. (f) As (e) for the synoptic scale and the time series of Fig. 9. (g) Intraseasonal vs. synoptic in AM. (h) As (g) for AF.

**Figure S1** Principal component analysis of OLR anomalies over the "South American" sector, period NDJF 1979-2012. The first three modes are significant according to a scree-test. All spatial patterns are correlation maps with the principal component time series. Dashed curves show the 95% significance bound according to a Bravais-Pearson test. The variance explained by each mode is labeled in the figure.

**Figure S2** As Fig. S1 over the "Southern African" sector, with five modes retained as significant.

### Table Captions

**Table 1** Contingency table of the negative ( $[-\infty -1]$ ), neutral ( $[-1 1]$ ) and positive ( $[1 +\infty]$ ) scores between the American ("AM") and African ("AF") time series at the synoptic scale. The first line indicates the number of occurrences and the second line corresponding percentages.

**TABLE**

	<b>AM &lt; -1</b>	<b>-1 ≤ AM ≤ +1</b>	<b>AM &gt; +1</b>	<b>Total</b>
<b>AF &lt; -1</b>	143 3.6%	409 10.4%	49 1.2%	601 15.2%
<b>-1 ≤ AF ≤ +1</b>	406 10.3%	1962 49.5%	398 10.0%	2766 69.8%
<b>AF &gt; +1</b>	59 1.5%	369 9.3%	165 4.2%	593 15.0%
<b>Total</b>	608 15.4%	2740 69.2%	612 15.4%	3960 100%

**Table 1** Contingency table of the negative ( $[-\infty -1]$ ), neutral ( $[-1 1]$ ) and positive ( $[1 +\infty[$ ) scores between the American (“AM”) and African (“AF”) time series at the synoptic scale. The first line indicates the number of occurrences and the second line corresponding percentages.

## FIGURES

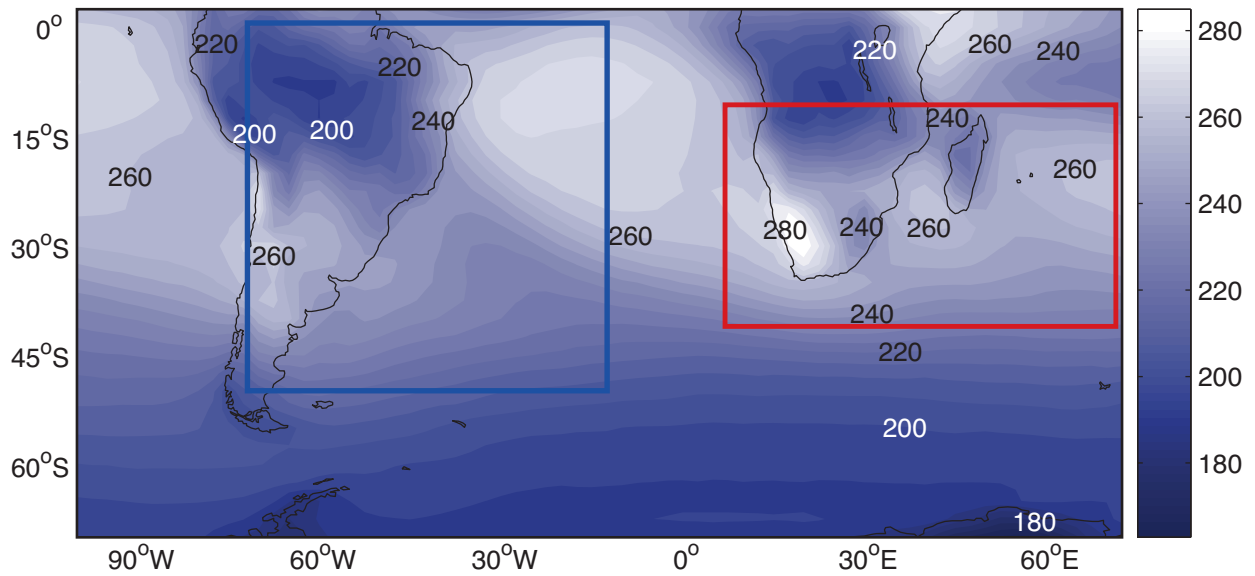


**Figure 1** Study domain for the "South American" sector (in blue: 50°S-0°, 70°W-10°W) and "Southern African" sector (in red: 40°S-10°S, 7.5°E-70°E), as well as the large region encompassing both domains. Shadings represent the austral summer (November through February) seasonal mean OLR field ( $\text{W m}^{-2}$ ).



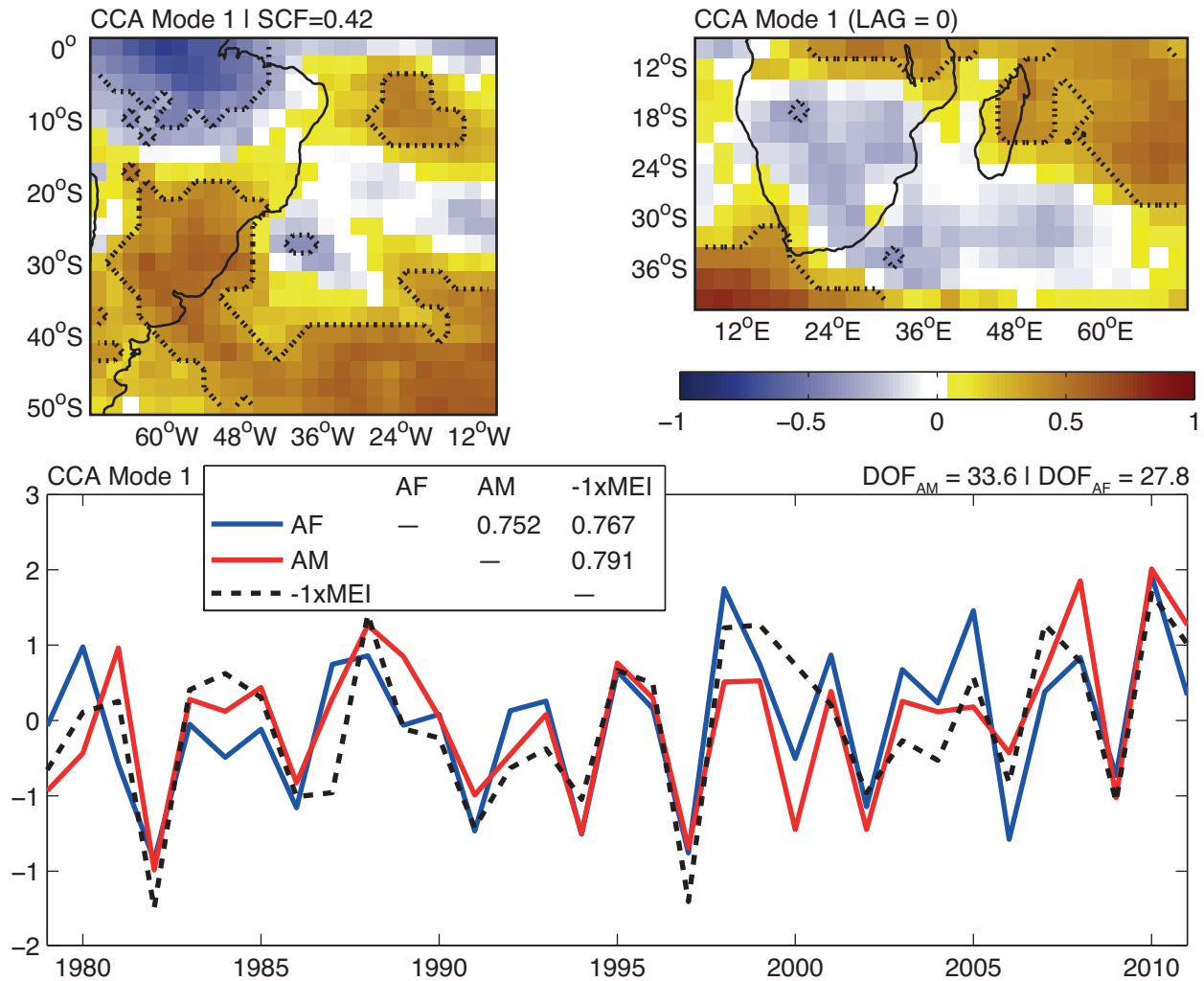


**Figure 2** Canonical correlation analysis of seasonal mean OLR co-variability at the interannual timescale between the "South American" and "Southern African" sectors, period NDJF 1979-2012. Upper panels: first mode of co-variability, displayed through heterogeneous correlation maps. Dashed curves show the 95% significance bound according to a Bravais-Pearson test. The squared coherence fraction (SCF) is labeled in the figure. Lower panel: associated time series, represented together with the seasonal mean Multivariate ENSO Index (MEI, multiplied by -1 for readability) over the same period. The correlation matrix between these time series and their actual number of degrees of freedom (considering possible serial auto-correlation) are indicated in the figure.

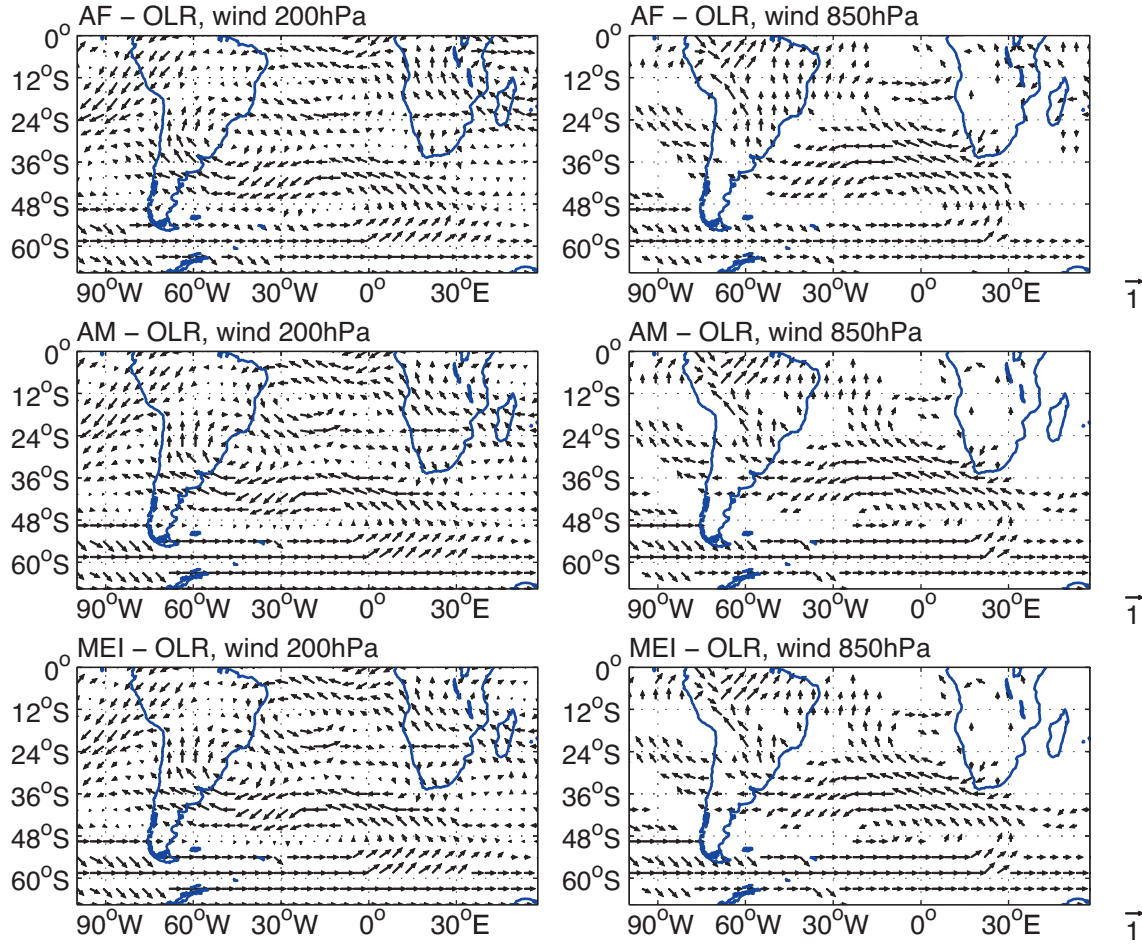
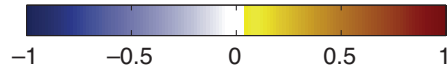
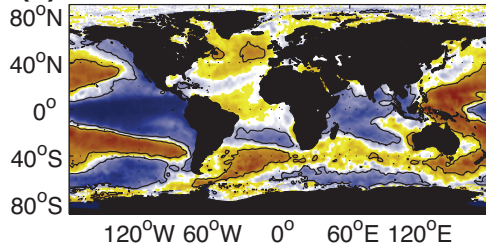


**Figure 3** Interannual correlations between the seasonal mean and horizontal wind at 200hPa (left-hand panels) and 850hPa (right-hand panels), and the three time series shown in Fig. 2. Only 95% significant correlations according to a Bravais-Pearson test are displayed.

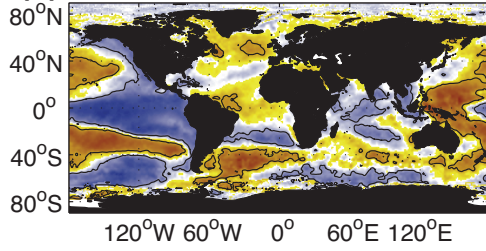
**Figure 4** (a) Interannual correlations between the seasonal mean SST and synchronous MEI, period NDJF 1979-2012. Black contours show 95% significant correlations according to a Bravais-Pearson test. (b, c) As (a) but for the AM and AF time series of Fig. 2, respectively. (d, e) As (b,c) but after removing linearly the influence of the synchronous MEI. (f-j) As (a-e) but correlations with the seasonal mean OLR field over the domain shown in Fig. 1.

→

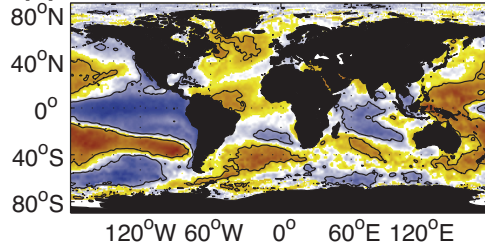
**(a)**  $-1 \times \text{MEI} - \text{SST}$



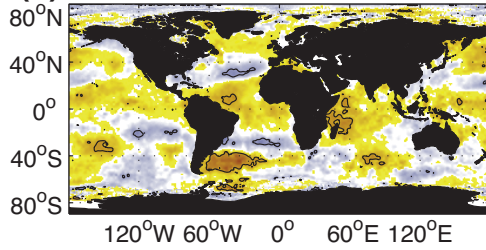
**(b)**  $\text{AM} - \text{SST}$



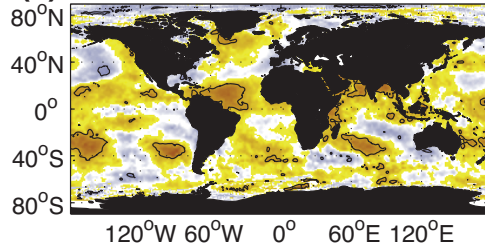
**(c)**  $\text{AF} - \text{SST}$



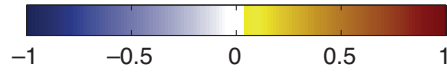
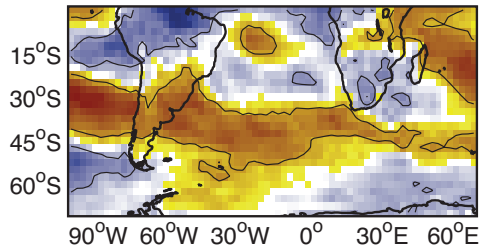
**(d)**  $\text{AM} - \text{SST} \setminus \text{MEI}$



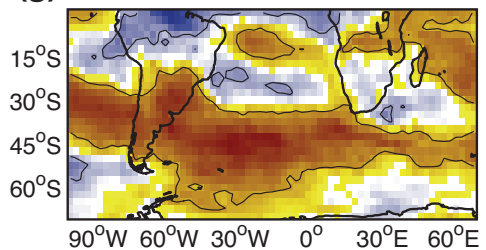
**(e)**  $\text{AF} - \text{SST} \setminus \text{MEI}$



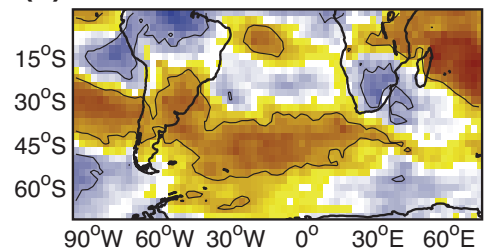
**(f)**  $-1 \times \text{MEI} - \text{OLR}$



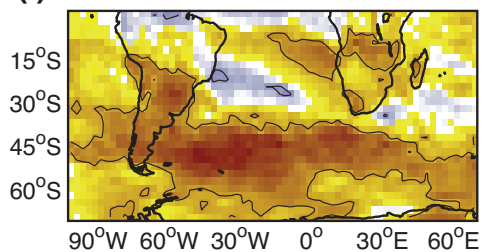
**(g)**  $\text{AM} - \text{OLR}$



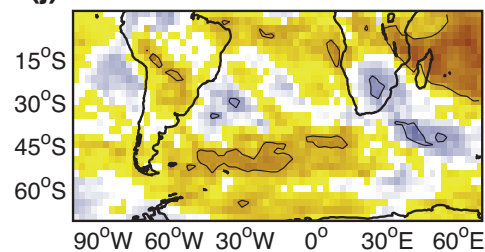
**(h)**  $\text{AF} - \text{OLR}$



**(i)**  $\text{AM} - \text{OLR} \setminus \text{MEI}$



**(j)**  $\text{AF} - \text{OLR} \setminus \text{MEI}$



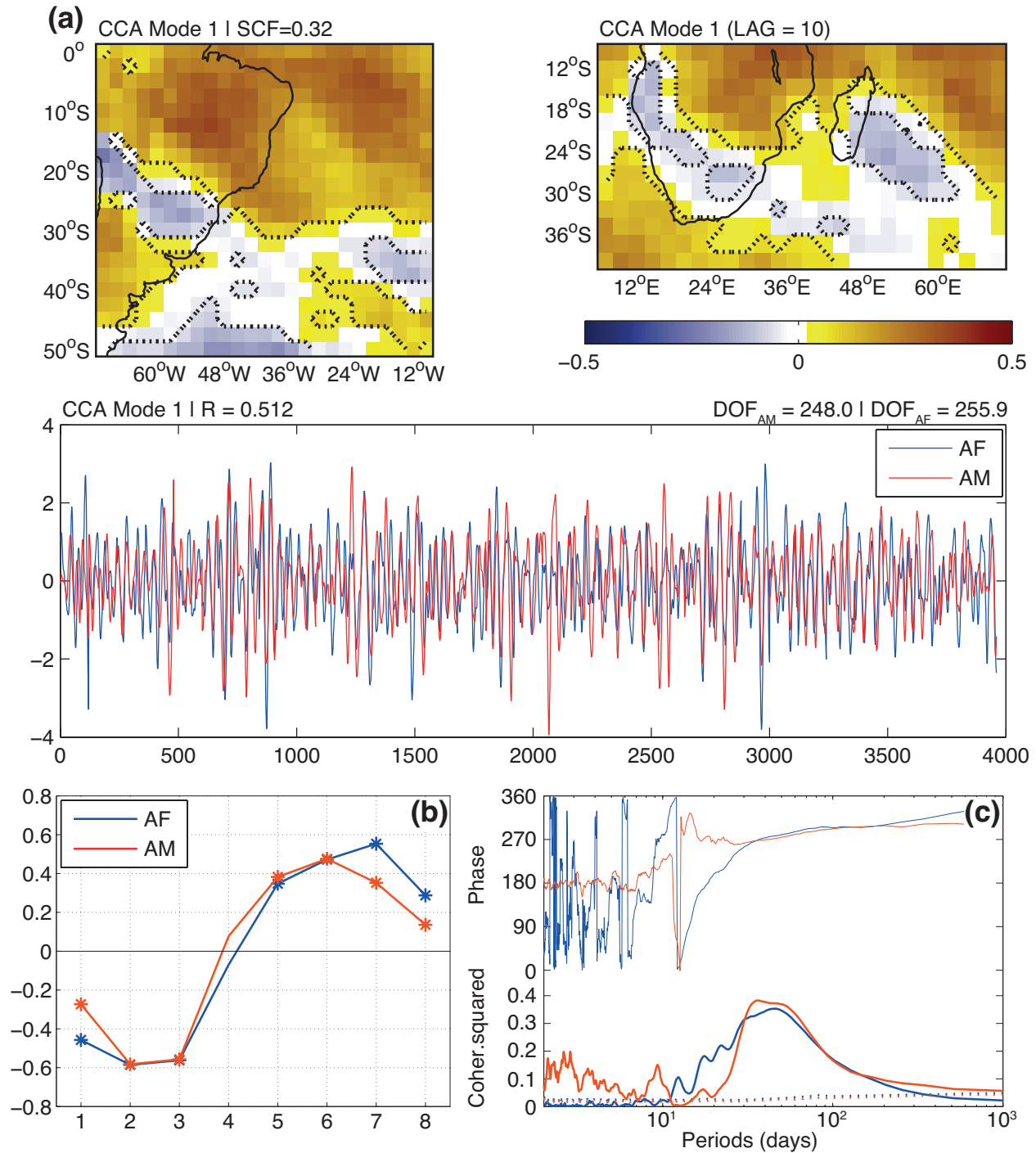
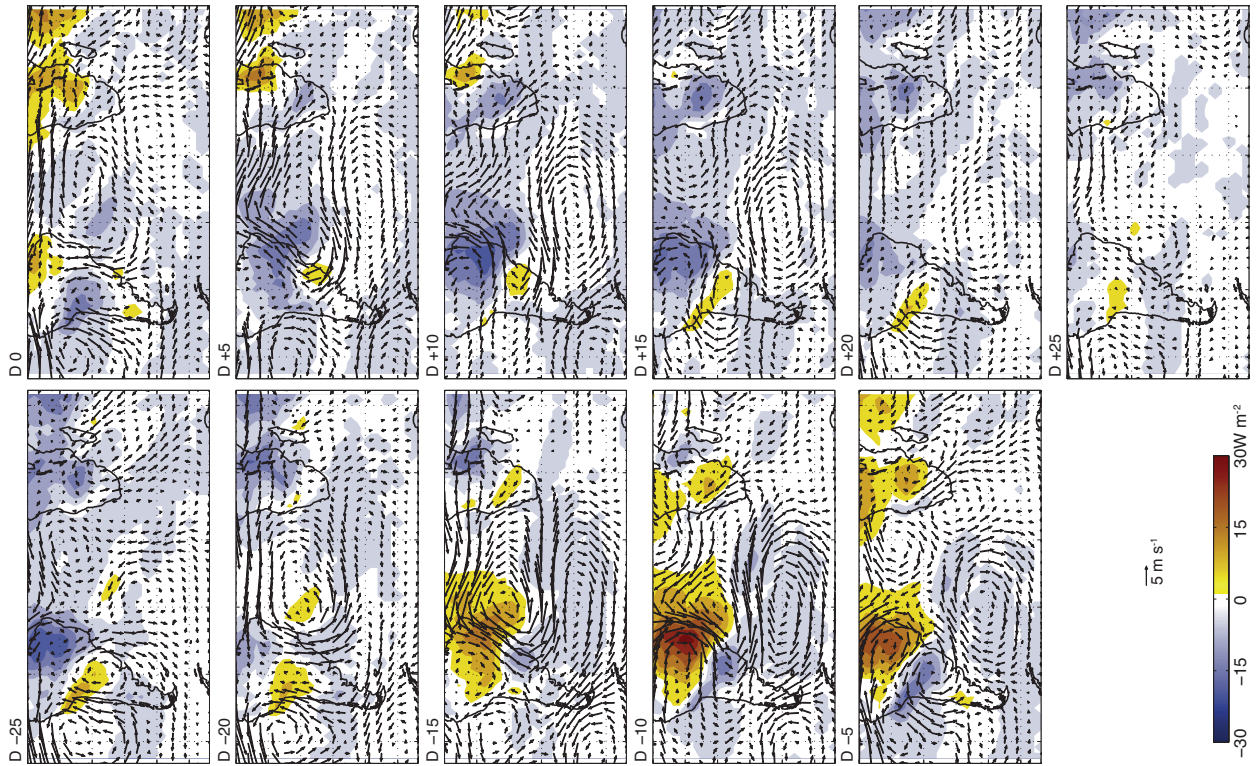
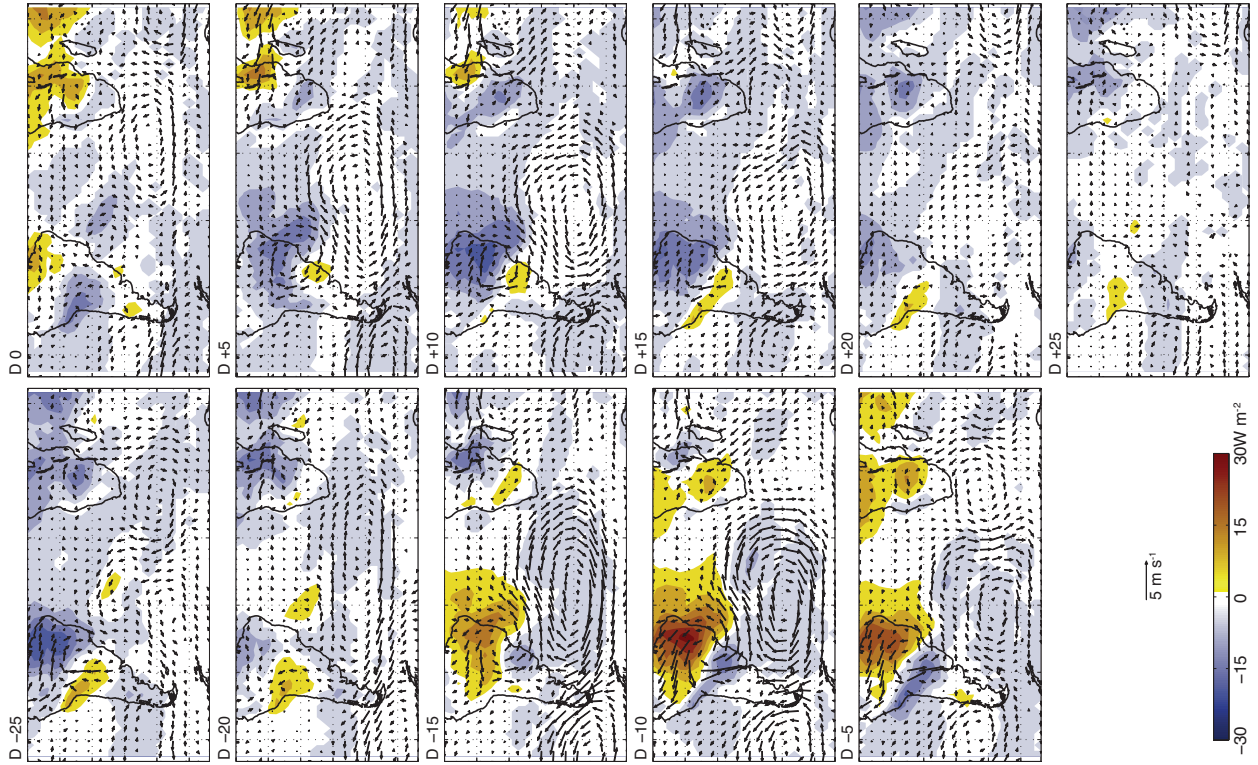


**Figure 5** (a) Canonical correlation analysis of 25-75-day bandpass filtered (intraseasonal) OLR co-variability between the "South American" and "Southern African" sectors, period NDJF 1979-2012. Upper panels: as Fig. 2, upper panels. A lag of 10 days is here applied between the two regions (South America leads Southern Africa by 10 days). Central panel: associated time series, their correlation and actual number of degrees of freedom. (b) Composite analysis of the CCA time series for the 8 phases of the MJO as defined by the RMM indices. Only days

characterized by an MJO amplitude larger than one standard deviation are considered. Asterisks denote 95% significant anomalies according to a  $t$ -test. (c) Cross-spectral analysis between the CCA time series and RMM1 index. All analyses are carried out on normalized data for the NDJF 1979-2012 period, with other months padded with zeros. Thick lines: squared coherence. Dashed lines: 95% level according to 1000 random time series obtained as permutations of the original time series, and having the same lag-1 serial correlation. Thin lines: phase relationship in degrees.

**Figure 6** Lead-lag composite analysis of daily OLR (shadings,  $\text{W m}^{-2}$ ), horizontal wind (vectors,  $\text{m s}^{-1}$ ) at 200hPa (left-hand panels) and 850hPa (right-hand panels), and opposite phases ( $>1$  standard deviation minus  $<-1$  standard deviation) of the AM time series shown in Fig. 5. Only 95% significant differences according to a two-tailed  $t$ -test (for OLR) and  $t^2$ -test (for the wind) are displayed. The  $t^2$ -test, also known as Hotelling test, is the multivariate generalization of the  $t$ -test. →





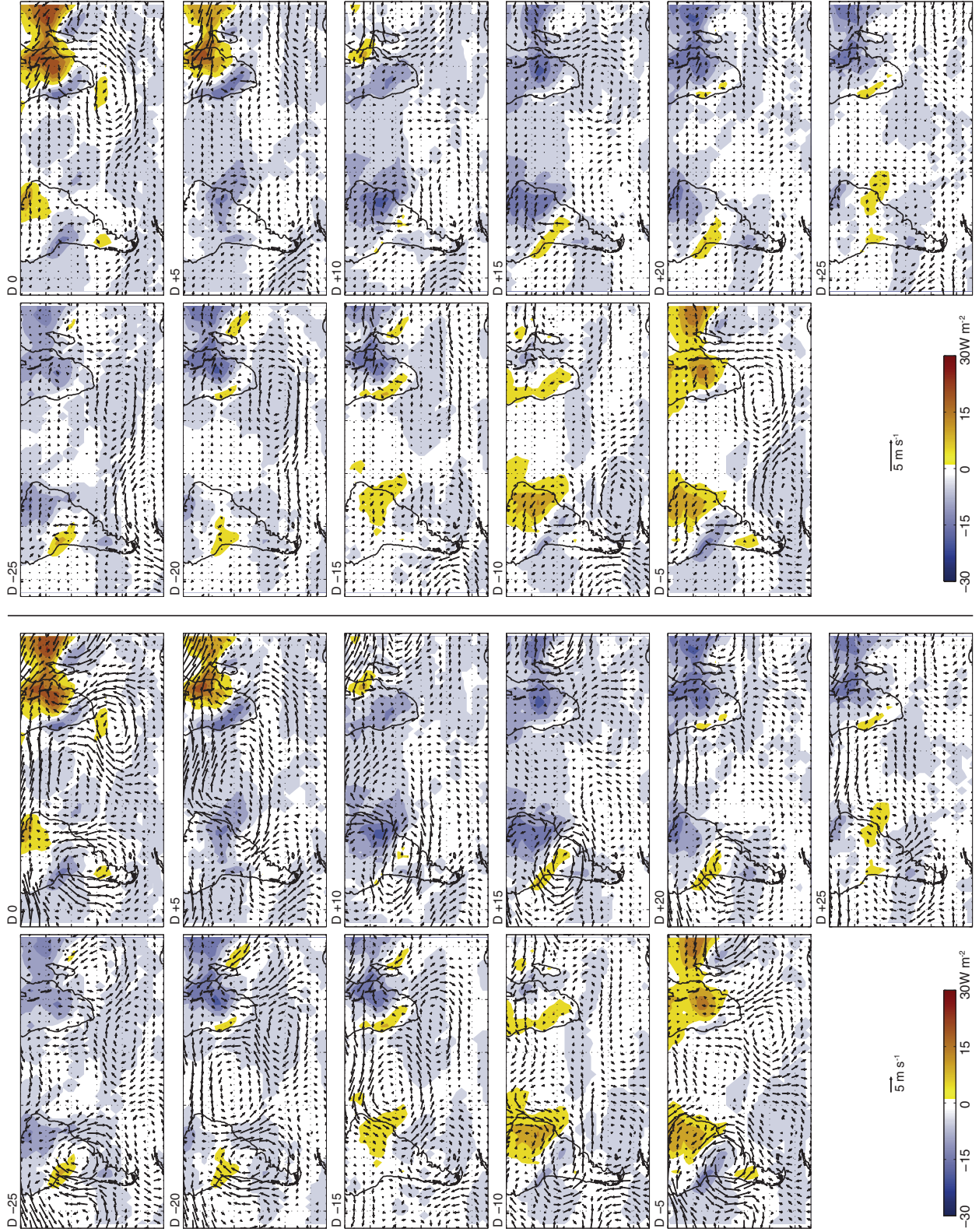


**Figure 7** As Fig. 6 but based on the AF time series of Fig. 5.



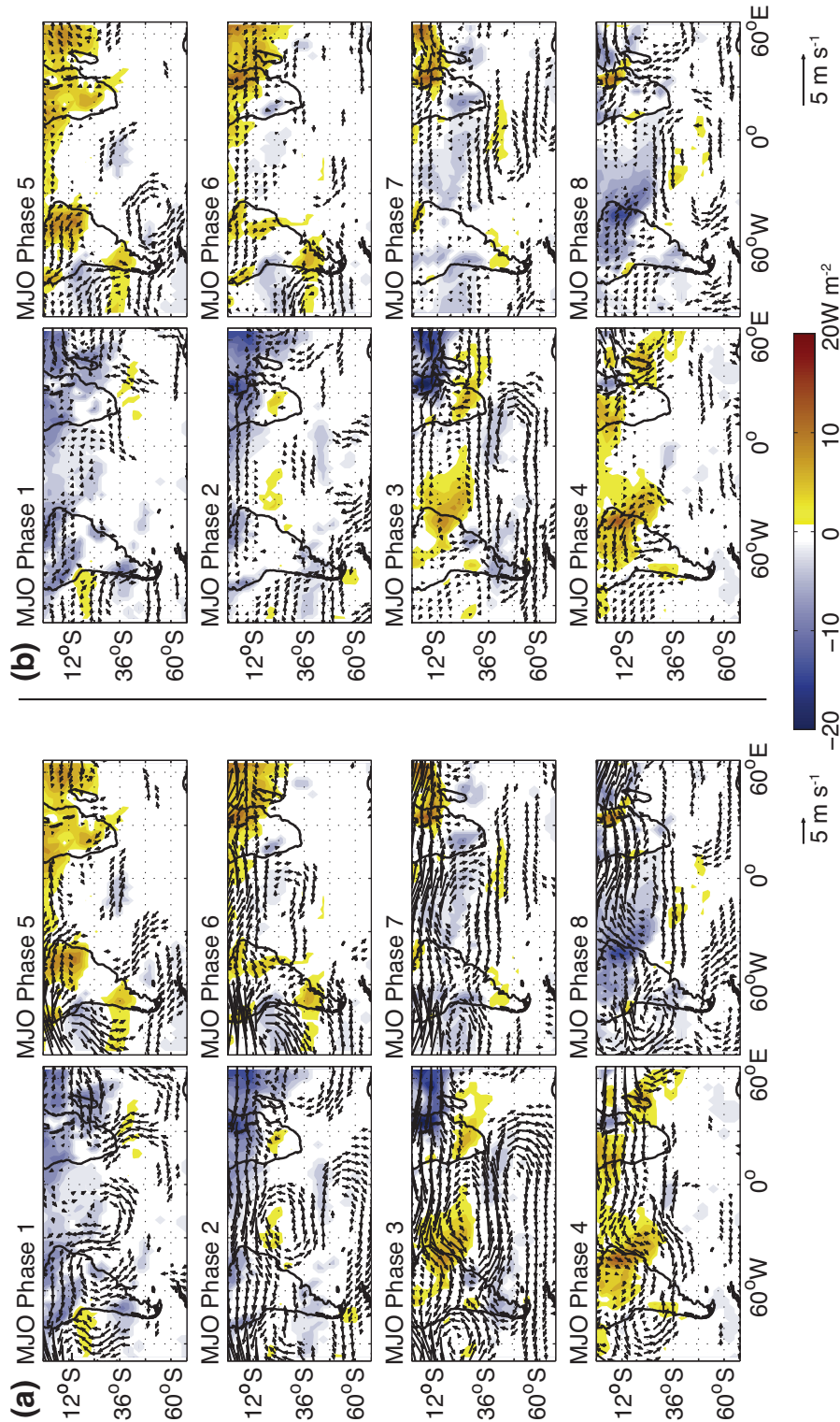


**Figure 8** Composite analysis of OLR (shadings,  $\text{W m}^{-2}$ ), horizontal wind (vectors,  $\text{m s}^{-1}$ ) at 200hPa (a) and 850hPa (b) for the 8 phases of the MJO as defined by the RMM indices. Significance is tested as for Fig. 6. Only days characterized by an MJO amplitude larger than one standard deviation are considered in the analysis.



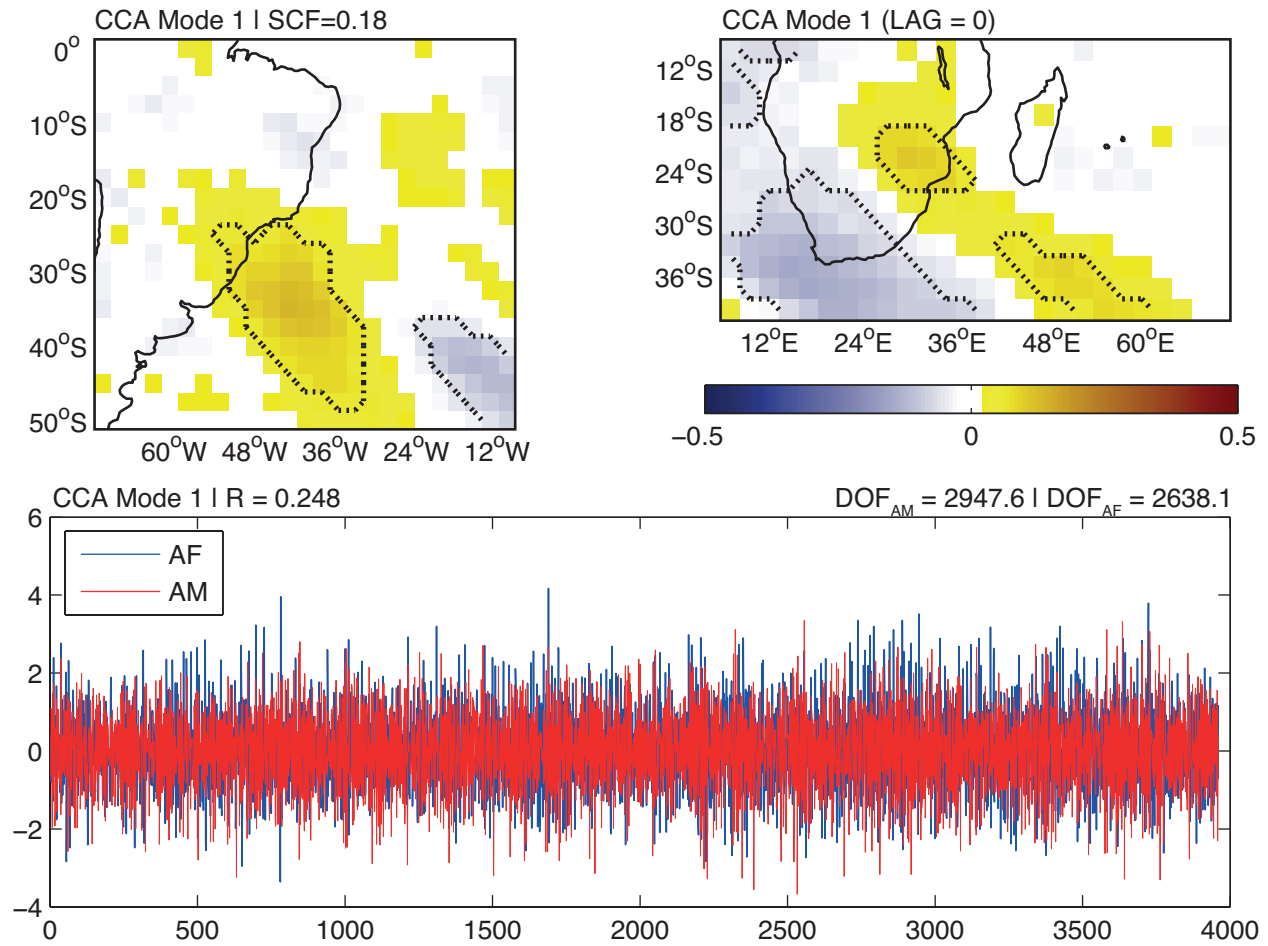


**Figure 9** As Fig. 5a but for 10-day highpass filtered (synoptic-scale) OLR. No lag (synchronous OLR fields) is applied between the two regions.

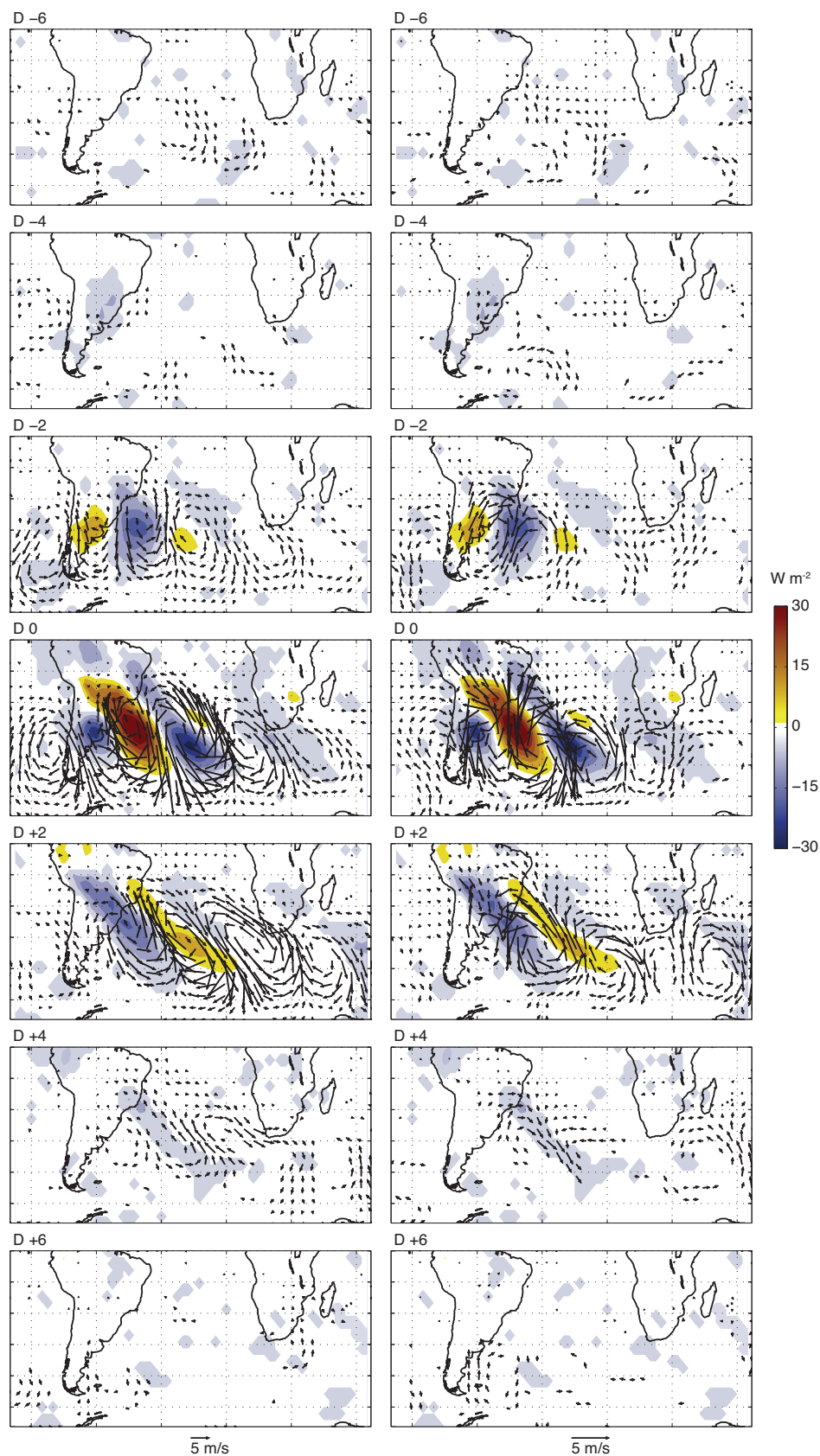


**Figure 10** As Fig. 6 but based on the AM time series of Fig. 9.

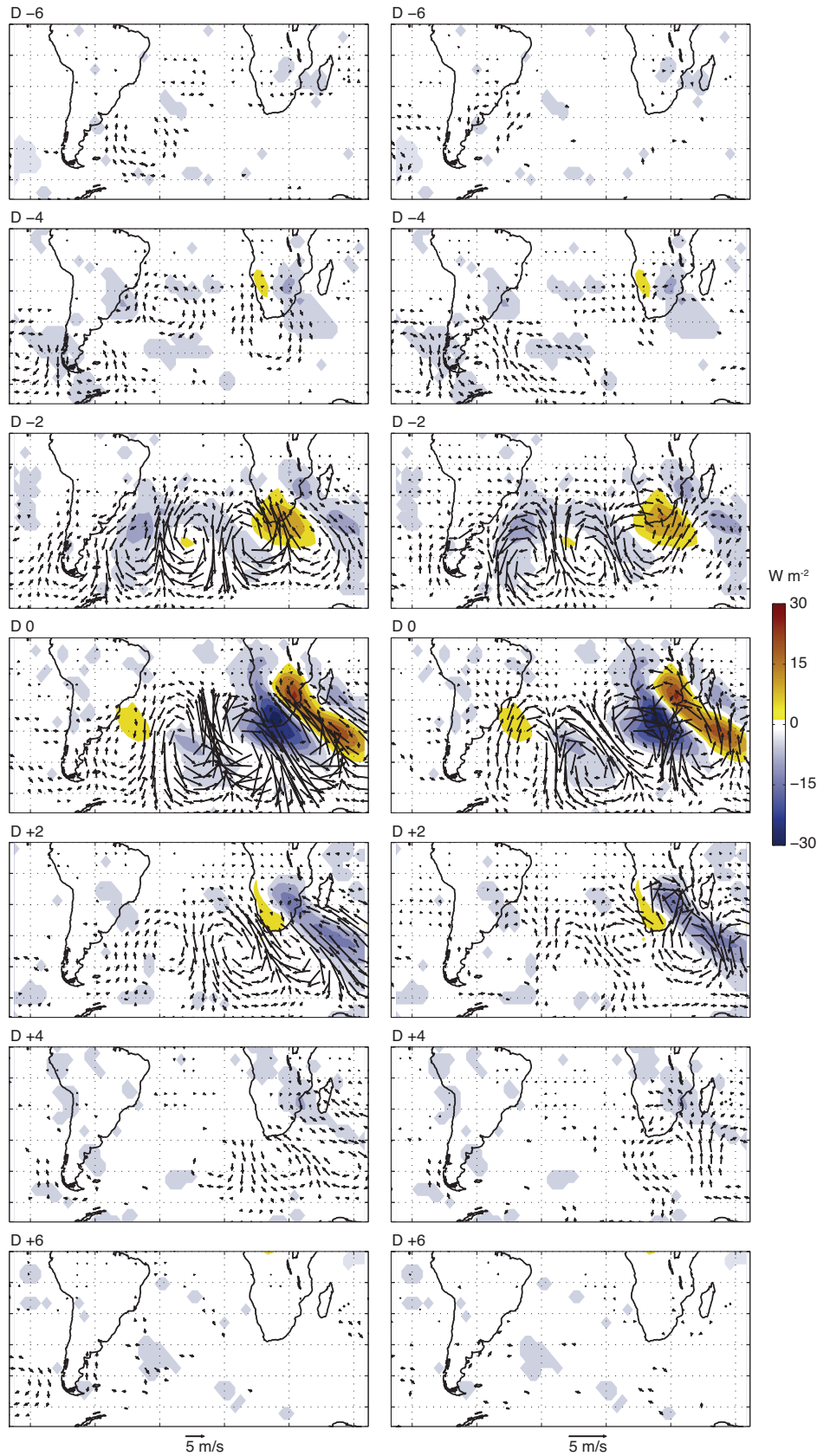


**Figure 11** As Fig. 6 but based on the AF time series of Fig. 9.

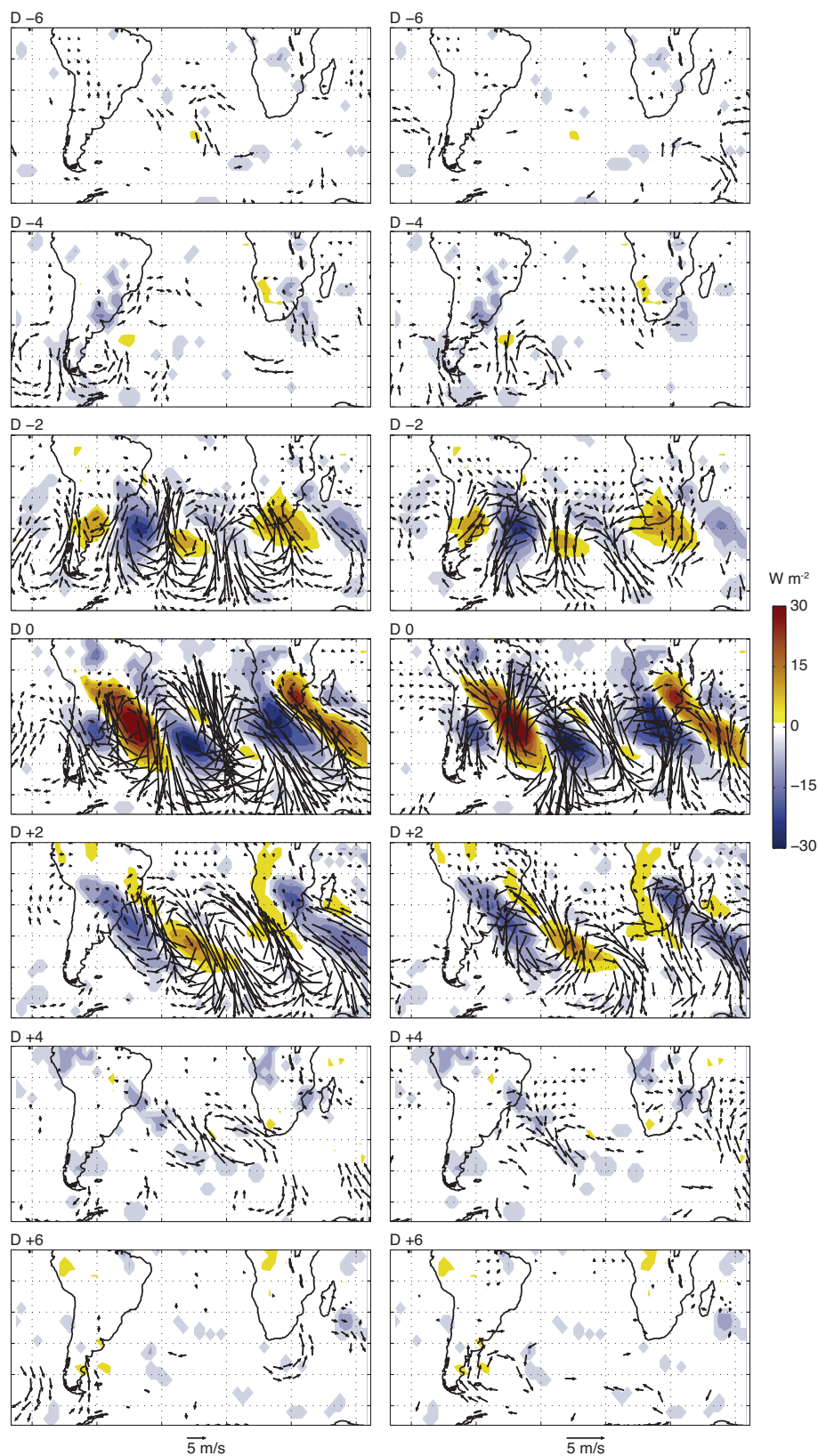


**Figure 12** As Fig. 6 but extracting the synchronous opposite phases of both AM and AF time series of Fig. 9 (i.e., “both positive” minus “both negative” events).

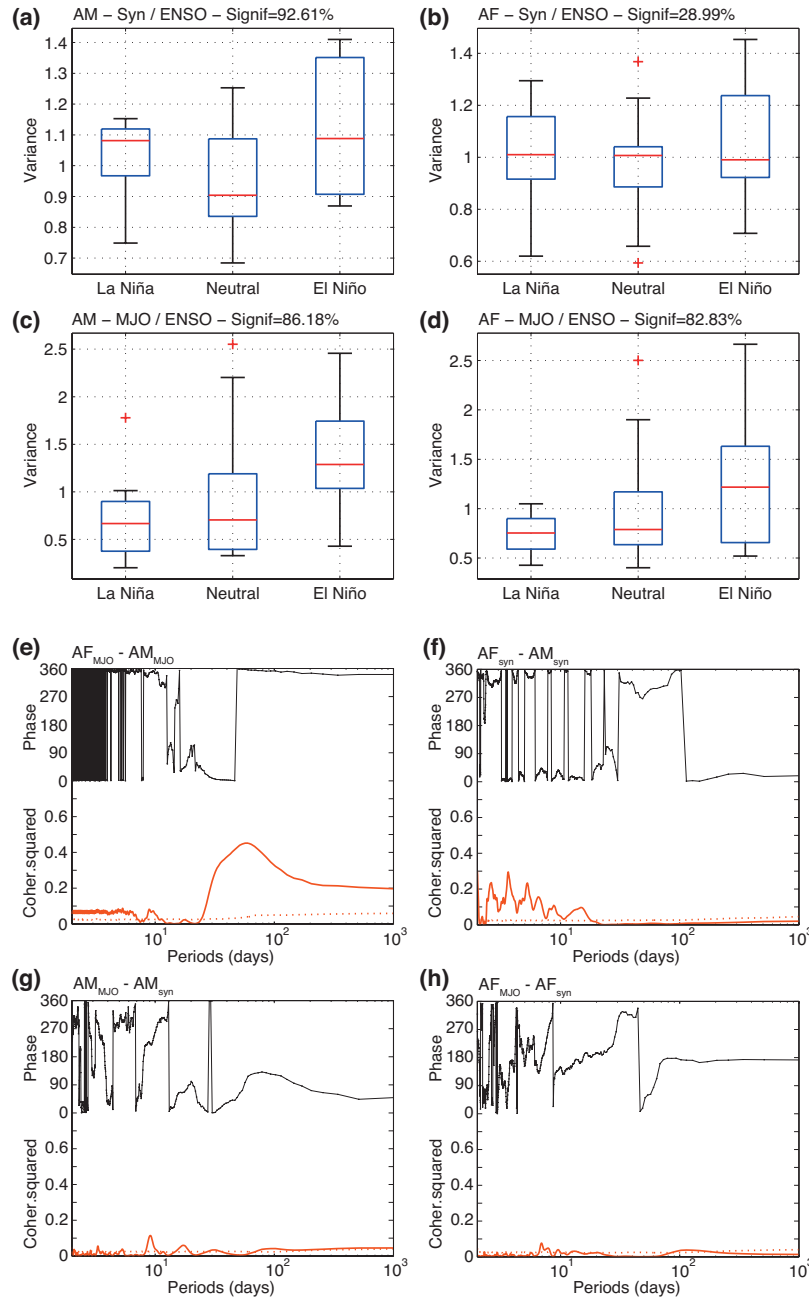


**Figure 13** Scale interactions between the interannual, intraseasonal and synoptic modes of variability and co-variability. (a) Interannual vs. synoptic in the AM region. Box-and-whisker representation of the seasonal variance of the AM time series for the synoptic scale, during El Niño, neutral ENSO and La Niña years. The boxes have lines at the lower quartile, median and upper quartile values. The whiskers are lines extending from each end of the box to show the range of the data. Outliers (outside of 1.5 inter-quartile range) appear as plus signs. (b) As (a) for the AF domain. (c, d) As (a,b) but for interannual vs. intraseasonal timescales. (e) AF vs. AM, intraseasonal scale. Cross-spectral analysis between the two time series of Fig. 6. (f) As (e) for the synoptic scale and the time series of Fig. 9. (g) Intraseasonal vs. synoptic in AM. (h) As (g) for AF.

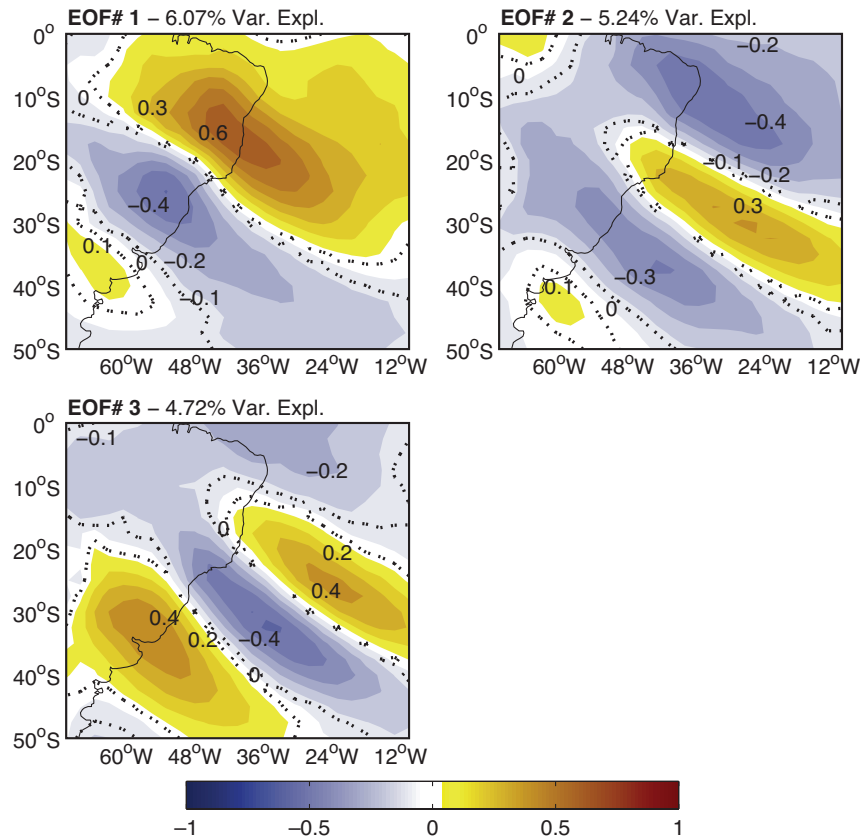


**Figure S1** Principal component analysis of OLR anomalies over the "South American" sector, period NDJF 1979-2012. The first three modes are significant according to a scree-test. All spatial patterns are correlation maps with the principal component time series. Dashed curves show the 95% significance bound according to a Bravais-Pearson test. The variance explained by each mode is labeled in the figure.

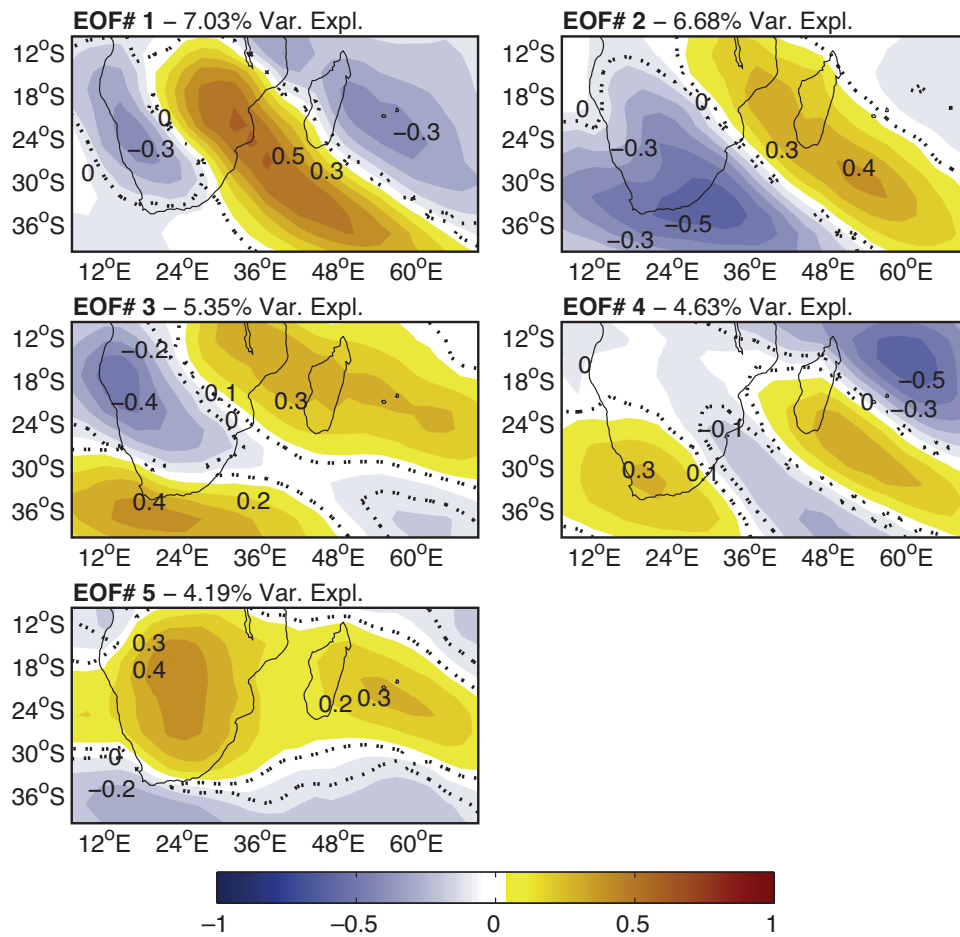


**Figure S2** As Fig. S1 over the "Southern African" sector, with five modes retained as significant.